HHS Public Access

Author manuscript

Water Resour Res. Author manuscript; available in PMC 2017 September 27.

Published in final edited form as:

Water Resour Res. 2016 May ; 52(5): 3324–3349. doi:10.1002/2015WR018224.

Recharge of low-arsenic aquifers tapped by community wells in Araihazar, Bangladesh, inferred from environmental isotopes

I. Mihajlov[*,#,1,2], **M. Stute**[1,3], **P. Schlosser**[1,2,4], **B. J. Mailloux**[3], **Y. Zheng**[1,5], **I. Choudhury**[6], **K.M. Ahmed**[6], and **A. van Geen**[1,*]

[1]Lamont-Doherty Earth Observatory of Columbia University, Palisades, NY 10964, USA

[2]Department of Earth and Environmental Sciences, Columbia University, New York, NY 10027, USA

[3]Barnard College, New York, NY 10027, USA

[4]Department of Earth and Environmental Engineering, Columbia University, New York, NY 10027, USA

[5]Queens College, City University of New York, New York, NY 11367, USA

[6]Department of Geology, Dhaka University, Dhaka 1000, Bangladesh

Abstract

More than 100,000 community wells have been installed in the 150–300 m depth range throughout Bangladesh over the past decade to provide low-arsenic drinking water (<10 μg/L As), but little is known about how aquifers tapped by these wells are recharged. Within a 25 km^2 area of Bangladesh east of Dhaka, groundwater from 65 low-As wells in the 35–240 m depth range was sampled for tritium (^3H), oxygen and hydrogen isotopes of water ($^{18}O/^{16}O$ and $^2H/^1H$), carbon isotope ratios in dissolved inorganic carbon (DIC, $^{14}C/^{12}C$ and $^{13}C/^{12}C$), noble gases, and a suite of dissolved constituents, including major cations, anions, and trace elements. At shallow depths (<90 m), 24 out of 42 wells contain detectable ^3H of up to 6 TU, indicating the presence of groundwater recharged within 60 years. Radiocarbon (^{14}C) ages in DIC range from modern to 10 kyr. In the 90–240 m depth range, however, only 5 wells shallower than 150 m contain detectable ^3H (<0.3 TU) and ^{14}C ages of DIC cluster around 10 kyr. The radiogenic helium (^4He) content in groundwater increases linearly across the entire range of ^{14}C ages at a rate of 2.5×10^{-12} ccSTP ^4He g^{-1} yr^{-1}. Within the samples from depths >90 m, systematic relationships between $^{18}O/^{16}O$, $^2H/^1H$, $^{13}C/^{12}C$ and $^{14}C/^{12}C$, and variations in noble gas temperatures, suggest that changes in monsoon intensity and vegetation cover occurred at the onset of the Holocene, when the sampled water was recharged. Thus, the deeper low-As aquifers remain relatively isolated from the shallow, high-As aquifer.

[*]Corresponding authors: imihajlov@gmail.com, avangeen@ldeo.columbia.edu.
[#]I.M. now at: Geosyntec Consultants, Huntington Beach, CA 92648, USA

AGU index terms

Groundwater hydrology; Stable isotope geochemistry; Chemistry of fresh water; Radioisotope geochronology; Water management

Keywords

Tritium; Radiocarbon; Noble gas temperatures; Arsenic; Bangladesh; Groundwater dating

1. Introduction

Arsenic is a naturally occurring toxic metalloid that is released from sediment to groundwater under anoxic conditions that prevail in the low-lying river and delta plain aquifers of South and Southeast Asia [Ravenscroft et al., 2009; Fendorf et al., 2010]. The majority of the rural population in Bangladesh, as in several other countries in the region, rely on privately-installed shallow tubewells for their drinking water supply. However, a large proportion of these wells contain As concentrations of >10 μg/L, exposing tens of millions of Bangladeshis and >100 million people throughout South and SE Asia to the harmful effects of As, including multiple forms of cancer, cardiovascular disease, and diminished childhood intellectual function [Smith et al., 2000; BGS/DPHE, 2001; Wasserman et al., 2004; Ravenscroft et al., 2009; Argos et al., 2010].

Exploiting the knowledge that peak As concentrations in the Bengal Basin are usually located 20–40 m below ground level (bgl), and that deeper, orange-colored sediments of Pleistocene origin usually host low concentrations of dissolved As in groundwater [BGS/DPHE, 2001; van Geen et al., 2003; Ravenscroft et al., 2005; McArthur et al., 2008; Fendorf et al., 2010], non-governmental organizations and government agencies have installed >100,000 deep (150–300 m bgl) wells in Bangladesh alone to mitigate the As poisoning [Ahmed et al., 2006; van Geen et al., 2007;; Michael and Voss, 2008; Burgess et al., 2010; DPHE/JICA, 2010; Ravenscroft et al., 2013]. Deeper wells appear to be an effective and available alternative for low-As drinking water supply in the short term [Ravenscroft et al., 2013; 2014]. As this source of low-As drinking water is increasingly pumped for urban supply and a cone of depression is developing around Dhaka [Hoque et al., 2007], several studies have raised concerns about the sustainability of its use. The possibility of vertical leakage of high-As and organic laden shallow groundwater due to irrigation pumping has been evaluated for deeper wells with basin-scale models under the assumption that in the coming decades pumping for irrigation purposes might switch to the currently safe aquifers at depths >150 m bgl [Michael and Voss, 2008; Burgess et al., 2010; Radloff et al., 2011].

The low-As aquifers have been characterized as Pleistocene in age or older, and their sediments have likely been flushed of labile As and/or organic carbon that could fuel the reductive release of As [BGS/DPHE, 2001; Ravenscroft et al., 2005]. The flushing presumably occurred due to a sequence of sea level lowstands, resulting in deep river channel incisions, larger horizontal hydraulic gradients in aquifers compared to the present, and consequently faster groundwater flow during the Pleistocene [Goodbred and Kuehl, 2000b; McArthur et al., 2008]. However, depth is a poor predictor for aquifers that are

systematically low in As in the Bengal Basin because of the large hydrogeological heterogeneity of the delta [van Geen et al., 2003; Zheng et al., 2005; McArthur et al., 2008; Fendorf et al., 2010].

Previous studies have identified transitional aquifers, boundaries of which vary in depth, where groundwater As is low, but the residence times and other hydrogeochemical features may resemble those of the high-As aquifer, and “deep” aquifers typically found at greater depths that contain much older groundwater [Aggarwal et al., 2000; BGS/DPHE, 2001; Hoque and Burgess, 2012]. In this study, the transitional aquifer is referred to as “shallow” low-As aquifer (<90 m bgl), whereas the deeper aquifers are split into “intermediate” (90–150 m bgl) and “deep” (>150 m bgl) categories. These definitions account for the drilling method used for well installations, as well as the government’s Department of Public Health Engineering standard definition of wells deeper than 150 m as deep [van Geen et al., 2015; Choudhury et al., 2016]. The shallow aquifer designates the low-As aquifer that extends beneath the depth of peak As concentrations [van Geen et al., 2003] to the depth of ~90 m bgl, within the reach of the traditional hand-flapper installation method [Ali, 2003; Horneman et al., 2004]. Wells in the intermediate aquifer (90–150 m bgl) can no longer be installed by the hand-flapper technique but are shallower, and therefore less expensive to install, than the typical deep wells (>150 m bgl).

Despite concerns about the status of the deep aquifer [Hoque et al., 2007; McArthur et al., 2008; Michael and Voss, 2008; 2009a; b; Burgess et al., 2010; Fendorf et al., 2010; Mukherjee et al., 2011; Radloff et al., 2011], and a few reports of well failures [Aggarwal et al., 2000; van Geen et al., 2007] or presumed incursions of As and/or organic matter from Holocene aquifers [McArthur et al., 2011; Mukherjee et al., 2011], relatively little is known about the basic hydrology of the low-As aquifers, including flow patterns and mean residence times. Groundwater dating, primarily by ^{14}C in dissolved inorganic carbon (DIC), has typically covered large areas with sparsely spaced data points [Aggarwal et al., 2000; BGS/DPHE, 2001; Fendorf et al., 2010; Majumder et al., 2011]. The available data indicate that low-As groundwater at depths >120 m bgl, and in certain locations at depths of only ~30 m bgl [Zheng et al., 2005], might be >10 kyr old. Previous studies that integrated spatial observations of deep groundwater ages have argued that deep aquifers are recharged by long flowpaths originating from the basin margins [Majumder et al., 2011; Hoque and Burgess, 2012], and such a conceptual model of flow has been successfully tested by the models of Michael and Voss [2008]. However, the above studies did not use multiple tracers and did not consider the potential impact of climate change at the Pleistocene to Holocene transition about 12 kyr ago.

In this study, we report tritium (^{3}H) concentrations from 65 low-As wells ranging in depth between 35–240 m bgl in a 25 km^2 area approximately 20 km east of Dhaka, Bangladesh. Radiocarbon ages based on DIC ^{14}C data from a subset of 38 wells are interpreted using groundwater chemistry records, compared to a noble gas dating technique, and linked to the stable isotopic ratios in groundwater ($^{2}H/^{1}H$, $^{18}O/^{16}O$, $^{13}C/^{12}C$DIC). Field procedures and measurement techniques, litholog collection, and groundwater sampling and analyses for ^{3}H, $^{13}C/^{12}C$ and $^{14}C/^{12}C$ (in DIC and dissolved organic carbon, DOC), major cations, anions, Si, P, As, Mn, Fe, DIC and DOC concentrations, $^{2}H/^{1}H$, $^{18}O/^{16}O$, and noble gases

are described in Section 2. The results of these measurements and analyses, along with the ^{14}C age correction models and the noble gas model used to calculate recharge temperatures and radiogenic He, are presented in Section 3. Section 4 provides a discussion of the main results, including groundwater chemistry and age/residence time estimates at different depths of the low-As aquifers. The isotopic ratios of the deepest and oldest samples are also placed into the context of deglaciation in early Holocene. The implications of our findings for the sustainability of deep, low-As aquifers are discussed before concluding the study in Section 5.

2. Methods

2.1. Field area and sampling campaigns

The study was conducted in Araihazar upazila approximately 20 km east of the capital, Dhaka, in an area described by van Geen et al. [2003] where the majority of shallow wells (mostly <30 m deep) exceed 50 μg/L As dissolved in groundwater (Fig. 1). This area has also seen decreasing water levels at depth (Fig. 2) likely due to depressurization caused by deep pumping in Dhaka, resulting in a growing downward vertical hydraulic gradient between the shallow, high-As and deeper, low-As aquifers. Recent data indicated that this gradient generally ranges from 0.01 to 0.03 in the study area, but averaged as high as 0.16 over the last year of measurements at the location shown in Figure 2. The present study focuses on 65 low-As wells (<10 μg/L As, except three wells with 10–29 μg/L As) that were installed in the depth ranges of 35–88 m bgl (n = 42), and 104–153 m bgl (n = 10), and 205–238 m bgl (n = 13) (Fig. 1, Table 1). A subset of the studied wells (n = 20 at the shallow depth, 35–90 m bgl, n = 6 at intermediate depth, 90–150 m bgl, and n=13 at depths >150 m bgl) was sampled for a broad series of chemical parameters, referred to here as extensive sampling, whereas the remaining wells were only sampled for ^{3}H and/or water stable isotopes (^{18}O and ^{2}H).

Extensive well sampling in 2010 and 2011 was performed mostly from community wells used for drinking, including 18 community wells (CW) and 13 Water Aid Bangladesh (WAB) wells. CWs were installed at depths 35–152 m bgl by Dhaka University in 2001–2004 [van Geen et al., 2007] to provide access to As-safe water in the most severely affected villages within the study area. Some CWs were sampled twice for $^{14}C_{DIC}$ (2010 and 2011) and two or three times for ^{3}H (2006, 2010, 2011); all measured values are reported. WAB wells, installed later in 2010 by the NGO Water Aid Bangladesh over a broader area, are deeper (>200 m bgl) and cluster towards the eastern end of the study area. A set of 8 monitoring wells installed in the intermediate depth range (35–88 m bgl) was also extensively sampled, including M1.5 (2011), DI4 (2008), and the deepest wells from multi-level well nests A–G (2003). Well DI4 was sampled before the *in situ* study of As sorption on low-As aquifer sediments reported by Radloff et al. [2011], whereas some results of the sampling of wells A–G were also previously reported [Zheng et al., 2005; Stute et al., 2007; Dhar et al., 2008; Mailloux et al., 2013]. All well screens were made of slotted PVC and ranged in length from 6.1 m (20 ft) at WAB wells to 3.0 m (10 ft) at CWs and 0.9–1.5 m (3–5 ft) at all other locations.

2.2. Well purging and field measurements

Well sampling was conducted using a submersible pump producing a flow rate of 5–10 L/min (Typhoon 12-V standard pump, Groundwater Essentials), or by utilizing a hand pump when a submersible pump could not be used due to well construction, i.e. for all WAB wells, with the exception of no. 24030. Tritium sampling of community wells in 2006 was also conducted using the existing hand pump in order to avoid contamination. Three borehole volumes were purged out of a well before sample collection. Electrical conductivity (EC), temperature (T), and pH were monitored by probes in a flow-through portable chamber (MP 556, YSI, Inc.) during purging with a submersible pump and stabilized before sampling. Alkalinity was also measured in the field using standard Gran titrations [Gran, 1952]. Electrodes (EC and pH) were calibrated on site before collecting the first sample of the day, and the flow cell was taken off the line before sample collection to prevent cross-contamination between wells. For WAB wells sampled by hand pumps, EC and pH were measured in an overflowing bucket, which may have introduced a systematic error in pH due to degasing of CO_2 from the splashing water. For these wells, pH was calculated (denoted by # in Table S1) from the field-measured alkalinity values (not affected by CO_2 degassing) and the total DIC measured at the Woods Hole NOSAMS facility. DIC samples for radiocarbon measurements were collected into glass bottles directly from the hand pump, without splashing, and immediately capped.

2.3. Groundwater sampling and elemental analysis by ICP-MS and IC

Samples for major cation (Na, K, Mg, Ca), Si, P, and trace element (As, Fe, Mn) analysis were collected without filtration into 25 mL HDPE scintillation vials with conical polyseal caps (Wheaton, Fisher Scientific) and later acidified to 1% HCl (Optima, Fisher Scientific). Previous work demonstrated that the well screens in Bangladesh typically provide sufficient filtration without introducing artifacts associated with syringe filtration, such as the removal of Fe and PO_4 by rapid ferrihydrite precipitation [Zheng et al., 2004], and that delayed acidification in the lab does not affect the results [van Geen et al., 2007]. The samples were analyzed for Na, K, Mg, Ca, Si, P, As, Fe, and Mn by high-resolution inductively coupled plasma–mass spectrometry (HR ICP-MS) on a single-collector VG Axiom [Cheng et al., 2004] to a precision of ±10% or better. Accuracy of the results was checked against an internal laboratory reference standard and also found to be within <10% of the expected values.

Unacidified samples for anion analyses were collected in parallel with cation and trace element samples. The samples were maintained refrigerated until analysis except for the duration of travel from Bangladesh to USA. The concentrations of Cl, F, Br, and SO_4 were determined on a Dionex ICS-2000 ion–chromatograph (IC) with an IonPac AS18 analytical column and an AG18 guard column (Thermo Scientific) using a self-regenerating KOH eluent. A standard was run after every 8–10 samples to ensure accuracy of the measurements, and several samples were analyzed in duplicates or triplicates to confirm analytical precision (typically <5% for Cl, <10% for SO_4, and 5–15% for Br and F).

2.4. Sampling and analysis of stable isotopes in water ($H_2{}^{18}O/H_2{}^{16}O$ and $H^2H^{16}O/H_2{}^{16}O$ ratios)

Stable isotope samples were collected in 60 mL glass bottles with polyseal lined caps. Measurements of samples collected in 2003 (wells A-G), 2004 (several CWs), and 2008 (DI4) were performed at the Environmental Isotope Laboratory of the University of Waterloo with a precision of ±0.1‰ ($H_2{}^{18}O/H_2{}^{16}O$ ratio expressed as $\delta^{18}O$) and ±1‰ ($H^2H^{16}O/H_2{}^{16}O$ ratios expressed as δ^2H). Stable isotope measurements on samples collected in 2010 and 2011 (CWs, WABs, and M1.5) were performed on a cavity ringdown (CRD) laser spectrometer at Lamont-Doherty Earth Observatory (L2130-*i* Isotopic H_2O, Picarro, Santa Clara, CA) with a precision better than 0.05‰ ($\delta^{18}O$) and 0.25‰ (δ^2H). All values are reported in the δ-notation as ‰ deviation from Vienna Standard Mean Ocean Water (VSMOW).

2.5. Sampling and analysis of ^3H and noble gases (He, Ne, Ar, Kr, Xe, and $^3He/^4He$)

Groundwater recharged after the onset of surface testing of nuclear weapons can be detected by the presence of elevated tritium (^3H), a radioactive isotope of hydrogen released during the tests that began in 1950s and peaked in the early 1960s [e.g., Weiss et al., 1979; Weiss and Roether, 1980], provided that adequate detection limit of ^3H is achieved [Eastoe et al., 2012]. Samples for ^3H were collected in 125 mL glass bottles with polyseal caps and analyzed at Lamont-Doherty Earth Observatory's Noble Gas Laboratory using the ^3He ingrowth technique [Clarke et al., 1976; Bayer et al., 1989; Ludin et al., 1998]. The detection limit of the ^3H analyses was 0.05–0.10 TU (1 TU corresponds to a $^3H/^1H$ ratio of 10^{-18}), with a precision of ±0.02–0.16 TU (Table 1). Noble gas samples were collected in copper tubes (~1 cm outer diameter) that contain ~19 cm^3 of groundwater. Concentrations of He, Ne, Ar, Kr, and Xe isotopes were measured by mass spectrometry [Stute et al., 1995] with typical analytical precisions of ±2% for He and $^3He/^4He$, and ±1% for Ne, Ar, Kr, and Xe. The system was calibrated with atmospheric air standards and water samples equilibrated with atmospheric air at known temperature and pressure.

The measured concentrations of noble gases (He, Ne, As, Kr, and Xe; Table 3) were processed through a sequence of inverse numerical models to estimate the temperature of each groundwater sample at the time of recharge based on the known equilibrium solubilities of noble gases in water [Aeschbach-Hertig et al., 1999; Peeters et al., 2003]. Besides fitting the equilibrium temperature, the models also account for gases in excess of the atmospheric equilibrium concentrations due to trapped bubbles, commonly referred to as "excess air". The excess air component is either fitted without any fractionation from the atmospheric air (assuming complete dissolution of the bubbles) or with various processes and degrees of fractionation. A constant salinity of 0 and atmospheric pressure of 1013 mbars were assumed for the model calculations. After the best fit was found for observed Ne, Ar, Xe, and Kr concentrations, the predicted He concentration was calculated according to the same model [Aeschbach-Hertig et al., 1999; Peeters et al., 2003]. Any ^4He in excess of that amount was reported as "excess He" and is considered a radiogenic input from the radioactive decay processes, hence it can also be named "radiogenic He". If the input of radiogenic He comes primarily from the aquifer sediments, it can be proportional to the age or residence time of groundwater under the following assumptions: (1) the aquifer matrix

and release rates of He from the sediment are fairly homogeneous and constant along the flowpaths; (2) little degasing loss occurs; and (3) no confounding effects of deep crustal He degassing occur [Torgersen and Clarke, 1985].

The model output also included a χ^2 probability that the model is consistent with the data. Low χ^2 probabilities are considered a reasonable criterion to reject the models, with <1% often used and <5% being a very strong criterion to reject the run. Errors of the modeled temperature and excess He were estimated by a numerical propagation of the experimental uncertainties through the inverse procedure with data sets generated by Monte Carlo simulations [Aeschbach-Hertig et al., 1999; Peeters et al., 2003].

2.6. Sampling and analysis of $^{14}C/^{12}C$ and $^{13}C/^{12}C$ in DIC and DOC

Samples for radiocarbon ($^{14}C/^{12}C$) and carbon stable isotopic ($^{13}C/^{12}C$) measurements on dissolved inorganic carbon (DIC) and dissolved organic carbon (DOC) were collected in 125 mL or larger glass bottles with polyseal caps and immediately “poisoned” with 0.1 mL of saturated mercuric chloride solution. All carbon isotopic measurements were performed at the National Ocean Science Accelerator Mass-Spectrometer (NOSAMS) facility at the Woods Hole Oceanographic Institution following standard protocols [Elder et al., 1997]. Ratios of $^{13}C/^{12}C$ are reported as $\delta^{13}C_{VPDB}$ in ‰ deviations from the Vienna Pee Dee Belemnite standard, with a typical error of ±0.1‰. Radiocarbon data ($^{14}C_{DIC}$ and $^{14}C_{DOC}$) are reported as fraction modern (FM), “modern” being defined as 95% of the AD 1950 radiocarbon concentration of NBS (National Bureau of Standards) Oxalic Acid I normalized to $\delta^{13}C_{VPDB}$ of −19‰ [Olsson, 1970]. FM values were normalized for C isotopic fractionation to a value of $\delta^{13}C_{VPDB} = -25$‰. Errors in FM measurements are shown in Table 2 and range from 0.0012 to 0.0041 FM. Concentrations of DIC and DOC were also reported by NOSAMS for the samples collected in 2010 and 2011 (±2% precision), including some CWs and most WAB wells. For the remaining samples, DIC concentration was calculated from alkalinity and pH values measured in the field (in a flow cell). Where both are available, DIC concentrations calculated from the field data and those reported by NOSAMS are typically in agreement within <10%.

2.7. Lithologs

Drill cuttings were collected at 2–5 ft (0.6–1.5 m) intervals from 49 of the 52 wells ≤152 m deep (i.e. all except deep WAB community wells) and were used to calculate the total clay +silt thickness above the well screen (Table 1). The thicknesses of all clay and silt layers encountered in the litholog were added, except for the ground surface clay/soil, as this layer does not play a role in separating the high-As shallow aquifers from the low-As shallow aquifers. We use a depth of 90 m (300 ft) to distinguish shallow private wells installed within a day by a handful of drillers using the manual hand percussion (or “hand-flapper”) method from intermediate wells in the 90–150 m depth range which require a larger team working for several days using a manual rotary drilling-direct circulation method with a double-acting (“donkey”) pump [Ali, 2003; Horneman et al., 2004]. Lithologs for the wells <90 m deep (i.e. the shallow low-As wells) are more reliable in terms of recording the presence of clay layers than lithologs collected with the donkey pump, which are more likely

to miss clay layers. Sand color at the depth of filter intake was noted for each well, regardless of the installation depth.

3. Results

3.1. Tritium (^{3}H), radiocarbon (^{14}C), and arsenic

With the exception of three wells that contain 10–29 μg/L As (Fig. 3b) and tap the shallow aquifer (<90 m bgl), all community wells met the WHO guideline for As of 10 μg/L at the time of sampling despite many years of use [van Geen et al., 2007]. Of the 65 wells sampled for ^{3}H, 8 had elevated ^{3}H concentration greater than 0.3 TU, indicating a significant contribution of groundwater recharged within the past 60 years (Fig. 3a and Table 1). All 8 of these wells were screened at depths ≤65 m bgl and contained <3 μg/L As, where measured. Another set of 23 wells contained low ^{3}H concentrations (0.10–0.27 TU) at least at one time of sampling, 21 of which were detectable at the 95% confidence level (0 TU was not within the range of 2σ, twice the analytical error). Most (16) of the 21 wells containing low-level, detectable ^{3}H clustered in the shallow aquifer, whereas only 5 such samples were found in the intermediate aquifer (90–150 m bgl) and none at depths >150 m bgl. The number of samples with detectable ^{3}H paired to concurrent samples with valid noble gas measurements was limited to 3 wells in the shallow aquifer, thus ^{3}H/^{3}He ages were not calculated. Results from the wells sampled two or three times between 2006–2011 (Table 1) showed no temporal trends in ^{3}H concentrations over this time period.

Radiocarbon concentrations in dissolved inorganic carbon (DIC) range from 0.26 to 1.12 FM in groundwater from shallow depth <90 m bgl (Fig. 3c and Table 2). Deeper than 90 m, a uniform radiocarbon signature of 0.25–0.31 FM is observed in intermediate and deep aquifer DIC. Within the shallow aquifer, some $^{14}C_{DIC}$ values fall within the range of those observed in intermediate and deep aquifer groundwater, but only 3 of these samples have a consistent intermediate/deep aquifer signature across various parameters measured in this study (A7, A8, and C5, labeled by pink fill in Fig. 3 and thereafter). These samples come from a shallow outcrop of the confined Pleistocene aquifer in the northwest of our study area [van Geen et al., 2003]. On the other end of the spectrum, samples from 4 wells with the highest $^{14}C_{DIC}$ (0.93–1.12 FM) also have ^{3}H >2 TU (Fig. 3c), confirming that groundwater recharged since the nuclear weapon testing began in the late 1940s reached these shallower wells, carrying the so-called “bomb” ^{14}C and ^{3}H with it. The remaining shallow aquifer samples (below ~0.9 FM $^{14}C_{DIC}$) contain a lower range of ^{3}H concentrations (<0.3 TU).

3.2. Radiocarbon dating

3.2.1. ^{14}C age corrections—Three groundwater age estimates were determined for each sample on the basis of radiocarbon data (Fig. 3d and Table 2). The ^{14}C half-life of 5730 yr (the “Cambridge half-life”) was used to generate the maximum radiocarbon age, denoted as the uncorrected ^{14}C age (“UC ^{14}C age”). This age assumes the initial ^{14}C concentration of DIC or DOC at recharge to be 1 FM and assumes an evolution of DIC without any carbon reservoir corrections:

$$\text{UC } {}^{14}\text{C age (yr BP)} = \frac{5730 \text{ yr}}{ln2} * ln\left(\frac{1}{\text{FM } {}^{14}\text{C}}\right) \quad (1)$$

This approach might be appropriate for particulate organic material, but the initial ^{14}CDIC is rarely 1 FM, as total DIC is formed by the dissolution of soil CO_2 and resident soil carbonates in an open system before the system closes off from the contact with vadose zone carbon sources [Fontes and Garnier, 1979]. Whereas the soil CO_2 is a product of oxidation of plant remains, the ^{14}C activity of which is often close to that of atmospheric CO_2, soil carbonates usually have a lower ^{14}C activity. One way to estimate the initial ^{14}C activity of DIC is to empirically relate $^{14}C_{DIC}$ to observed ^{3}H concentrations (Fig. 4), following Verhagen et al. [1974]. This approach yielded an estimate of initial $^{14}C_{DIC}$ of 0.90 FM for our data set, close to the value of 0.87 FM used by Hoque and Burgess [2012] in their Bengal Basin ^{14}C work and also close to the fixed value of 0.85 FM applied in the "Vogel" model [Vogel and Ehhalt, 1963; Vogel, 1967]. Therefore, the corrected radiocarbon age, or the "C_1 ^{14}C age", is adjusted for the initial $^{14}C_{DIC}$ formed under open system conditions, but not for any subsequent dissolution of carbonates along the flowpath:

$$C_1 \ {}^{14}\text{C age (yr BP)} = \frac{5730 \text{ yr}}{ln2} * ln\left(\frac{0.09}{\text{FM } {}^{14}\text{C}}\right) \quad (2)$$

Finally, the minimum ^{14}C age was calculated from the C_1 ^{14}C age by estimating the maximum possible contribution of carbonate dissolution along the flowpath to the total DIC and its final ^{14}C concentration, after the system was closed with respect to gas exchange in the vadose zone. This was achieved by using a simple isotopic mixing model based on the δ^{13}C of two end members: the initial DIC and carbonate minerals [Hoque and Burgess, 2012]. In order to make this the maximum possible correction for carbonate dissolution, the value used for the initial $\delta^{13}C_{DIC}$ was −25‰, in accordance with the values in Harvey et al. [2002] and Hoque and Burgess [2012], and appropriate for the dominance of ^{13}C-depleted C3 plants [Sarkar et al., 2009]. Similarly, to make this a minimum age, the carbonate minerals in the mixture were assumed to be of marine origin (δ^{13}C = 0‰) and free of radiocarbon. Thus, the minimum radiocarbon age – C_2 ^{14}C age – includes a correction for mixing of different carbon pools, similar to that of Ingerson and Pearson [1964], but with an added correction for initial $^{14}C_{DIC}$ of 0.90 FM:

$$C_2 \ {}^{14}\text{C age (yr BP)} = \frac{5730 \text{ yr}}{ln2} * ln\left(\frac{0.90}{\text{FM } {}^{14}\text{C}} * \frac{\delta^{13}\text{C}_{\text{DIC}}}{-25‰}\right) \quad (3)$$

None of the above ^{14}C age corrections account for isotopic fractionation effects during the isotopic exchange reactions of C species ($CO_{2(g)}$ to $CO_3^{2-}{}_{(aq)}$ equilibrium), which can have some impact on the final ^{13}C contents [Fontes and Garnier, 1979]. The above models also do not take into account the mineralization of groundwater DOC subsequent to the initial recharge, and the impact it might have on the budget of DIC radiocarbon. Lastly, the ^{14}C

ages were not calibrated to calendar years, as doing so would not be meaningful for dating of groundwater $^{14}C_{DIC}$ that is subject to as many uncertainties as presented above.

3.2.2. Calculated DIC ^{14}C ages—The shallow aquifer groundwater spans a wide range of DIC ^{14}C ages, calculated by all three methods, from modern in the high-^{3}H samples to 7–11 kyr in samples A7, A8, and C5 that resemble the deep aquifer (Fig. 3d and Table 2). In contrast, DIC ^{14}C ages of the intermediate and deep aquifer groundwater are greater and less variable when calculated by a single method, but as seen with the older samples in the shallow aquifer, variation of ages from 6 to 12 kyr exists between different methods of age calculation. The variability among different age calculation methods, and between samples from the shallow aquifer and pooled intermediate and deep aquifer samples, can visualized by the box plots (Fig. S2) that provide minimum, 1st quartile, median, 3rd quartile, and maximum values of the sample group. The ^{14}C age corrected for the initial DIC ^{14}C content of 0.90 FM (C_1 age), based on the empirical relationship between ^{3}H and ^{14}C, places the age of intermediate and deep groundwater samples within the 9–11 kyr range, with an average of 9,800 ^{14}C yr before present (BP). The maximum, uncorrected (UC) age would result in these samples being ~900 yr older on average (10,700 ^{14}C yr BP), whereas the additional correction for dissolution of carbonates along the flowpaths (C_2 age) would make them younger by ~2–3 kyr (average 7,300 ^{14}C yr BP). The corrections from UC to C_1 and C_2 ^{14}C ages had a similar effect on the shallow aquifer groundwater ages, thus shrinking their overall range and shifting the results towards younger ages with each correction.

3.3. Noble gas temperatures and radiogenic He

The model that best fits the noble gas data (Table 3) considers the equilibrium temperature, the amount of excess air, and the fractionation of excess air as variables in the simulation ("Taf-1" model). The fractionation of excess air is conceptualized as a partial equilibrium dissolution of the trapped air bubbles in a closed system, or the "CE" model [Aeschbach-Hertig et al., 1999; Peeters et al., 2003]. Some of the model results were rejected (Table 3) based on a low model probability and/or a high error in model temperature estimate (>1.5 °C error). At least some of the samples for which the model failed to converge suffered from degassing during sampling, as indicated by Ne concentrations below solubility equilibrium with the soil air ($<1.7\times10^{-7}$ ccSTP g^{-1}). Among the converged samples accepted for further analysis (16 out of 29 samples), model probabilities were well above the strict 5% threshold, except for CW42 with 3.4%, which still produced a reasonable fit (>1 %) and had the lowest model temperature error of the entire data set, thus the fit for this sample was accepted.

Current groundwater temperatures in the shallow low-As aquifer (Table S1) cluster around an average of 26.2 °C ± 0.3 °C (standard deviation), whereas the average temperatures in intermediate and deep groundwater are slightly higher at 26.7 ± 0.3 °C and 27.0 ± 0.4 °C, respectively. Temperatures calculated by the noble gas model (Table 3), also known as the noble gas temperatures (NGTs), represent groundwater temperatures at the time of recharge at the water table. In the shallow aquifer, NGTs vary between 22.0 and 25.9 °C (Fig. 5ab), with nine of the eleven converging samples clustering between 23.6 and 25.9 °C. Excluding the two outliers with NGTs close to 22 °C, average NGT of the shallow low-As samples is 24.5 °C (± 0.7 °C st. dev.), with the 95% confidence interval between 24.0 and 25.0 °C. The

two outliers lie outside the 95% confidence interval by more than double the model error of those samples, and one of them (sample A7 from 40.7 m depth) consistently exhibits the signature of deep aquifer tracers and chemistry. The shallow low-As aquifer 95% confidence interval of NGTs, nevertheless, lies below the temperatures currently measured in this aquifer, as well as below the available temperature measurements made by pressure transducers in very shallow, high-As wells in the study area (25.4 to 26.8 °C range, data not shown).

Intermediate and deep aquifer NGTs, pooled together, range from 21.2 to 24.7 °C with the average of 23.0 °C (± 1.6 °C st. dev.). The two lowest NGTs from this group are below any NGT observed in the shallow aquifer, and the 95% confidence interval of 21.5 to 24.4 °C is both wider and lower in absolute values relative to that of the shallow samples. There is no temporal trend in recharge temperatures, as NGTs plotted against the $C_1{}^{14}C$ age (Fig. 5b) do not have a statistically significant trend ($p = 0.19$).

The excess or radiogenic He, also estimated by the NG model, increases from ~0 to ~3×10^{-8} ccSTP g^{-1} in samples with ^{14}CDIC ranging from modern to ~0.25 FM, with the highest concentrations present in samples from the intermediate and deep aquifers and those with a low $^{14}C_{DIC}$ from the shallow aquifer (Fig. 5c). The relationship between the radiogenic He and the C_1 ^{14}C age (Fig. 5d) is linear, and corresponds to an empirical He accumulation rate of $^4He = 2.5\pm0.2\times10^{-12}$ ccSTP$g^{-1}yr^{-1}$ • ^{14}C age (yr) +/− 0.04×10^{-8} ccSTPg^{-1} ($R^2 = 0.94$, $p = 2\times10^{-8}$, samples from all depths were included in the regression). As a quality control, $^3He/^4He$ ratio was also measured. In samples that contain a high concentration of radiogenic He (up to ~35% of the measured He), $^3He/^4He$ ratio ranges between 0.9–1.1×10^{-6} (Table 3). The $^3He/^4He$ ratio in these samples falls below that of the remaining samples and below the ratio found in solubility equilibrium with atmospheric air (1.36×10^{-6}) because of the low $^3He/^4He$ ratio of radiogenic crustal He (~2×10^{-8}).

3.4. Chemical composition of groundwater

The great variability of ^3H and ^{14}C in the shallow aquifer compared to the intermediate and deep aquifers is matched by an even greater scatter in the shallow groundwater geochemical characteristics, such as pH, electrical conductivity (EC), alkalinity, DIC, Na, and Si concentrations (Fig. 6 and Table S1). In contrast, intermediate and deep aquifer groundwaters carry a more uniform signature of these parameters. In particular, deeper groundwater and the three shallow samples with deep ^3H and ^{14}C signatures cluster around lower values of pH (6.5–6.8), EC (0.3–1 mS/cm), alkalinity (1.7–3.0 mEq/L), DIC (3–4.8 mM), and Na (<50 mg/L) relative to most of the shallow aquifer samples, whereas Si concentrations are higher (55–70 mg/L). The concentrations of the remaining major cations (Ca, Mg, and K) and anions (Cl, SO_4) are variable and similar between the three aquifers (Fig. 6 and Table S1). One sample from the shallow aquifer (CW15) is particularly high in salinity/EC, with Cl and SO_4 concentrations of 629 and 24 mg/L, respectively.

Among the minor groundwater constituents, bromide concentrations remain ≤0.7 mg/L, where detectable (Fig. 9b). Fluoride concentrations are mostly <1 mg/L (Table S1), with intermediate and deep aquifer samples largely <0.4 mg/L. Two samples from the shallow aquifer (2–3 mg/L F) do exceed the WHO guideline of 1.5 mg/L. Fortunately, only one of

these high-F wells (CW18) is a drinking water source. Likewise, phosphate is generally below 0.6 mg/L P, except for one sample at 4.7 mg/L (Table S1). Finally, iron and manganese are highly variable in all three aquifers, with concentrations of up to 4 mg/L Fe (mostly <2 mg/L, but one sample has ~10 mg/L) and up to 1,400 μg/L Mn.

3.5. Environmental stable isotopes: $^{2}H/^{1}H$ and $^{18}O/^{16}O$ in water and $^{13}C/^{12}C$ in DIC

Most water stable isotope values (expressed as $\delta^{2}H$ and $\delta^{18}O$) fall on or near the global meteoric water line (GMWL: $\delta^{2}H = 8 \bullet \delta^{18}O + 10‰$), but many also plot to the right of this line as a result of evaporation and kinetic isotope fractionation (Fig. 7, Table 1). Virtually all intermediate and deep aquifer samples fall on the GMWL, indicating recharge by precipitation, and cluster around $\delta^{18}O$ values between −5 and −6‰ and $\delta^{2}H$ values between −30 and −40‰. The average isotope composition of modern precipitation in the area is similar to that observed in the intermediate and deep aquifer samples [Stute et al., 2007]. In contrast, stable isotopes of water in the shallow aquifer span a larger range of values, with nearly half of the samples impacted by some degree of evaporation before recharge, as judged by their distance from the GMWL. Several of the most evaporated samples were recharged in the last 60 years, as evidenced by their high ^{3}H concentrations (Fig. 7).

Carbon stable isotope values ($\delta^{13}C$) in DIC range between −15 and −22‰ in all three aquifers (Fig. 8, Table 2). The $\delta^{13}C_{DIC}$ values observed here fall in between those expected of oxidized OC from C3 plants (−28‰) and C4 plants (−13‰) in the Bengal Basin [Sarkar et al., 2009], under the assumption that the DIC was produced solely by the oxidation of bulk OC. Carbon isotopic fractionation process between dissolved CO_2 produced from OC in equilibrium with bicarbonate/carbonate ions can also account for some of the spread in observed $\delta^{13}C_{DIC}$ values, as $\delta^{13}C$ is 9–10‰ higher in carbonate ions [Fontes & Garnier, 1979].

A striking aspect of the stable isotopic data from intermediate and deep groundwater is the strong correlation of $\delta^{13}C_{DIC}$ with both $\delta^{2}H$ and $\delta^{18}O$ ($R^2 = 0.81$ for both isotopes, $\delta^{2}H$ vs. $\delta^{13}C_{DIC}$ shown in Fig. S1). Furthermore, all three stable isotopes are systematically correlated with ^{14}C in DIC of the intermediate and deep aquifer groundwater (Fig. 8; $\delta^{2}H$ not shown as it follows an identical pattern to that of $\delta^{18}O$). As ^{14}C FM increases, there is a consistent and statistically significant trend towards more negative values of all stable isotopes. The three shallow samples with characteristics of deeper groundwater also fit within the intermediate and deep aquifer trend.

In the shallow aquifer, however, an opposite trend from that in the deeper aquifers is noted: higher (more positive) values of $\delta^{13}C_{DIC}$, $\delta^{18}O$, and $\delta^{2}H$ are observed as $^{14}C_{DIC}$ increases toward modern values (Fig. 8). The trends are less sharply defined than for the deeper aquifers. In addition, the correlation of $\delta^{18}O$ (and $\delta^{2}H$) data with $^{14}C_{DIC}$ must be exaggerated in part by the evaporated nature of the most recently recharged samples with the highest ^{14}C content. The correlations between stable isotopes of the shallow aquifer are likewise less defined than in the deeper aquifers ($\delta^{2}H$ vs. $\delta^{13}C_{DIC}$ shown in Fig. S1).

4. Discussion

4.1. Penetration of recent recharge into the low-As aquifers

A considerable amount of recharge has occurred within the past 60 years in low-As portion of the shallow aquifer (<90 m bgl), as evidenced by detectable ^{3}H in 24 out of 42 sampled wells (57%). A subset of 8 wells (19% of the total) has particularly large contributions of bomb ^{3}H (>0.3 TU), as well as bomb ^{14}C (~1 FM), where both were measured (Tables 1 and 2). Variable ^{3}H concentrations were expected in the shallow aquifer in Araihazar given that even the high-As shallow aquifer (<20 m bgl) contains mixtures of older groundwater with post-bomb recharge [Stute et al., 2007]. Much of this recent recharge, as well as some of the older shallow aquifer groundwater, comes from a pool of surface water characterized by evaporative enrichment of stable isotopes (Fig. 7), such as stagnant ponds or rice fields that can hold flood water for months at a time [Stute et al., 2007]. In contrast, the intermediate (90–150 m bgl) and deep aquifer (>150 m bgl) groundwater was sourced directly from precipitation, and there is very little penetration of recent recharge to this depth. The presence of low, detectable ^{3}H concentrations (0.10–0.23 TU) in low-As portions of the intermediate aquifer (90–150 m bgl) does suggest a limited contribution of recent recharge at these depths. Using a conservative (low) value of 2–3 TU as a 100% benchmark, as any undiluted recharge since 1980 would now contain ~2–3 TU in the area, the maximum proportion of such a contribution can be 3–11%, and appears insufficient to alter isotopic composition of DIC in the intermediate aquifer. The highly variable ^{3}H and $^{14}C_{DIC}$ content of the shallow aquifer groundwater is matched by equally variable groundwater chemical properties (Figs. 3 and 6). In contrast, groundwater chemistry of the intermediate and deep aquifer is fairly uniform with consistently low EC, low alkalinity, low Na, high Si, and a Na/Cl ratio below that of the seawater (Figs. 6 and 9a).

The concentrations of ^{3}H and $^{14}C_{DIC}$ in groundwater provide a measure of vertical flow, not necessarily local flow, connecting the shallow aquifer to the surface and high-As aquifer. Whether the clay units are continuous and provide confinement could be important for the long-term fate of shallow low-As aquifers but difficult to ascertain. In an attempt to do so, we compared ^{3}H and $^{14}C_{DIC}$ concentrations to the thickness of overlying clay layers derived from the lithologs (Table 1). This is a simple parameter that presumably reflects the extent of vertical confinement of the aquifer. Overlying clay thickness turns out not to correlate well with either ^{3}H or $^{14}C_{DIC}$ concentrations in shallow low-As groundwater (Fig. 10). Where clay above the well screen is thicker than 20 m, measured ^{3}H values appear lower, but 4 of the 8 samples still contain detectable ^{3}H (0.1–0.2 TU) and thus receive some recent recharge from the surface. When samples containing ^{3}H concentrations >0.3 TU are excluded (yellow fill in Fig. 10), removing the locations with unusually rapid penetration of bomb ^{14}C from consideration, a weak negative correlation is revealed between the $^{14}C_{DIC}$ and the clay thickness (Fig. 10b), but this presumed longer-term trend is not statistically significant ($p = 0.075$). The lack of spatial correlations with local confining units is consistent with recent recharge arriving to the sampled locations via lateral flow and with the flow in the aquifer being mostly horizontal [Aziz et al., 2008]. The observed vertical communication of the shallow aquifer with the surface and high-As groundwater may occur in spatially limited areas of higher hydraulic conductivity where clay layers are thin or missing [McArthur et al.,

2010; Shamsudduha et al., 2015], and could be driven by local pumping that increases downward and lateral hydraulic gradients.

Notably, some samples from the shallow aquifer (A7, A8, C5) appear unaffected by recent recharge, as they have the deeper aquifer signature of low ^{14}C, high radiogenic He, low Na and low alkalinity (Figs. 3, 5, and 6). These wells are located in the NW corner of the study area, close to the southern edge of the uneroded Pleistocene uplands, known as the Madhupur Terrace [Goodbred and Kuehl, 2000b]. The protection of this part of the aquifer afforded by the interfluvial Madhupur paleosol might explain the Pleistocene signature of groundwater found there [McArthur et al., 2008], and the thickest clay layer among the reported lithologs is also found at well C5. This is an example of the area where local stratigraphy clearly limits groundwater flow between aquifers.

Another possible indicator of exchange between the surface and low-As aquifers might be the Cl/Br ratios in groundwater [McArthur et al., 2012]. Three samples from the shallow low-As aquifer stand out with a Cl/Br ratio higher than that of the seawater (yellow fill in Fig. 9b). Besides having an additional source of Cl, these samples have the highest measured ^{3}H concentrations and also contain excess SO_4 compared to the marine salt SO_4/Cl ratio (not shown), suggesting mixing with surface-derived wastewater. However, Cl/Br ratios of most samples are close to that of SW, indicating that all three low-As aquifers are largely unpolluted by wastewater [Ravenscroft et al., 2013]. Instead, Cl and Br are ultimately sourced from the ocean, via atmospheric aerosol inputs or via a low degree of mixing with remnant seawater from past coastline transgressions.

4.2. Groundwater residence time from radiocarbon ages

While mixing of groundwater with different ages can confound radiocarbon ages in the shallow aquifer, which vary from modern to ~10 kyr BP, ^{14}C ages in the intermediate and deep aquifers cluster at approximately 10 kyr BP. Given that the range of calculated residence times put the plausible date of intermediate and deep aquifer recharge to the onset of the Holocene, an issue worth considering is whether the ages need correction for dissolution of carbonates along the flowpath. The reported UC and C_1 ^{14}C ages of ~10–12 kyr BP do not include such a correction. The C_2 ^{14}C ages, however, include the additional correction for carbonate dissolution based on the observed $^{13}C/^{12}C$ ratios in DIC. This correction shifts estimated ages towards the mid-Holocene by 2–3 kyr, which could be significant in the context of changing climate conditions at the time of deeper aquifer recharge.

The relatively low pH, EC, and alkalinity (Table S1 and Fig. 6), as well as the molar ratio of Si to alkalinity of ~1 in the intermediate and deep aquifers (Fig. S1), suggest the predominance of silicate weathering in these aquifers, as do the weak, but significant, correlations of Ca and Mg with Si (not shown, $p < 0.04$ for both). In contrast, although Ca and Mg are the dominant cations at ~60–70 % of cation equivalence units in intermediate and deep groundwater (Fig. S1), their concentrations are negatively correlated with alkalinity and $^{13}C_{DIC}$ (Mg not shown; $p < 0.04$ for all correlations). This is the opposite of what would be expected from the dissolution of Ca or Mg-bearing carbonates in the system. Instead, the sum of Ca and Mg is well correlated with Cl (Fig. S1). Chloride dominates the

anion composition when Cl/alkalinity molar ratio is >1, i.e. in ~1/2 of the intermediate and deep samples, and is not related to carbonate chemistry.

The amount of acid-soluble carbonates found in either Holocene or the orange, Pleistocene sand in our field area is near or below the limit of quantification on Shimadzu carbon analyzer (0.01–0.02 weight %) [Mihajlov, 2014]. The Pleistocene sands are also typically low in Ca content [McArthur et al., 2008; van Geen et al., 2013; Mihajlov, 2014], presumably due to the more efficient aquifer flushing under the higher hydraulic gradients of the Pleistocene sea level lowstand [BGS/DPHE, 2001]. The Ca+Mg cation dominance and correlation with Cl in intermediate and deep groundwater (Fig. S1) might instead be related to the low Na concentrations and the low Na/Cl ratio through a cation exchange mechanism that depletes Na and enriches Ca and Mg in groundwater. This could occur during an episode of salinization of an aquifer previously well-flushed by freshwater [Ravenscroft and McArthur, 2004], such as at the onset of the Holocene. Rapid sea-level rise at the time could have caused a minor saltwater intrusion, limited in extent because intermediate and deep groundwater stable isotope ratios and Cl concentrations are not exceptionally high.

It follows from the above discussion that the dissolution of carbonates contributing older, ^{13}C-enriched DIC to groundwater may not be a correct explanation for the mutual correlations of lower $^{14}C_{DIC}$ with a more positive $\delta^{13}C_{DIC}$ and higher alkalinity in the intermediate and deep aquifers (Figs. 8 and S1). When a third dimension is added to the plot of $\delta^{13}C$ vs. ^{14}C age in DIC (Fig. 11b), it is clear that the high alkalinity samples are dispersed throughout the trend and not focused at more positive $\delta^{13}C$ values and older samples. Since these aquifers are dominated by silicate weathering, which does not add radiocarbon-free DIC to the system, ^{13}C correction for the ^{14}C age of DIC, as performed in the C_2 age calculation, appears unnecessary. The open system model (C_1 ^{14}C age) where the initial ^{14}C activity of DIC is empirically corrected to 0.9 FM appears sufficient to describe radiocarbon ages of the intermediate and deep groundwater and dates these samples to ~9–11,000 years BP (Table 2 and Fig. 3).

As a limitation to the reported radiocarbon ages, the influence of dissolved and particulate organic matter (DOC and POC) mineralization on the observed $^{14}C_{DIC}$ *after* groundwater was recharged and the system closed off from the vadose zone carbon inputs was not accounted for by the age calculations. In the intermediate and deep aquifers, younger DOC from the surface is unlikely to have been metabolized, as a very small proportion (3–10 %) of younger groundwater from the organic matter-rich Holocene aquifer penetrates to the intermediate depth and transport of reactive DOC has been shown to be a slow process [Mailloux et al., 2013]. Also, the DOC sampled in the shallow low-As aquifer is ~2 orders of magnitude lower in concentration than DIC (Table S1) and generally has the same or slightly older ^{14}C age than DIC (Table 2).

A possibility remains, however, that the consumption of resident DOC and POC from the Pleistocene (and older) sediments, coupled to reductive processes such as Fe, Mn, and SO_4 reduction or methanogenesis [Harvey et al., 2002], affects the ^{14}C content of DIC in addition to aging. Aging probably still dominates within our study area, however, given the systematic increase in radiogenic He with ^{14}C ages (Fig. 5d). In addition, methanogenesis is

unlikely to have played a major role in DIC genesis within our samples, as their DIC does not bear the characteristically enriched ^{13}C signature expected of the methanogenetic environments [Aravena et al., 1995; Harvey et al., 2002].

4.3. Radiogenic helium as a tracer of groundwater age

The linear relationship between C_1 ^{14}C age and the radiogenic He increases the confidence in the progression of ^{14}C ages of groundwater DIC (Fig. 5d), including also the shallow aquifer, even if the noble gas data did not constrain the absolute ^{14}C age. The slope of the relationship between ^{14}C age and radiogenic He is 2.5±0.2 $\times 10^{-12}$ ccSTP g^{-1}_{GW} yr^{-1} G for all samples combined, and it represents the ^{14}C-calibrated accumulation rate of He in groundwater due to the radioactive decay of U and Th from the surrounding sediment. To evaluate this result, the median value of the He accumulation rate in groundwater was calculated [Craig and Lupton, 1976; Torgersen, 1980] based on the U and Th concentrations found in the contemporary river sediment from the Ganges, the Brahmaputra and the Chittagong area rivers [Molla et al., 1997; Chowdhury et al., 1999; Granet et al., 2007; Granet et al., 2010; Chabaux et al., 2012], as well as for the average U and Th contents of the upper crust [Torgersen, 1989]. Assuming an aquifer porosity of 0.3, a sediment density of 2.75 g/cm^3, and a He release factor (lambda) of 1 (i.e. the release rate equals the production rate, [Torgersen and Clarke, 1985]), the calculated He accumulation rates are 4.9×10^{-12} and 4.1×10^{-12} ccSTP g^{-1}_{GW} yr^{-1} for the Bengal Basin sediment and the average upper crust, respectively, which is within a factor of <2 relative to the ^{14}C-calibrated rate determined from our data. The nearly 2-fold discrepancy may be explained by relative amounts of U and Th in sediments of different grain sizes; while coarser grained aquifer sands tend to by dominated quartz, U and Th concentrations are higher in the finer grained, clayey sediment. River sediments sampled in the above studies included both coarse and fine grained fractions, whereas our study was focused on aquifer settings. Moreover, our radiogenic ^4He accumulation rate is also within the range of rates ($1–3\times10^{-12}$ ccSTP g^{-1}_{GW} yr^{-1}) reported for a fluvial-deltaic formation in the Atlantic Coastal Plain of Maryland based on measured U-Th concentrations, ^{14}C ages, and ^{36}Cl ages [Plummer et al., 2012].

Our data from Bangladesh, as well as previous reports of the radiogenic He method [Plummer et al., 2012], suggest that the noble gas technique of He dating could possibly be applied to even older groundwater, such as that found at >200 m bgl in southern parts of Bangladesh with uncorrected ^{14}C ages of >20,000 yr BP [Aggarwal et al., 2000; Majumder et al., 2011; Hoque and Burgess, 2012]. The He dating could work provided that it is not affected by the He diffusing upward from deep, thermogenic natural gas deposits [Dowling et al., 2003], and if care is taken to cross-calibrate the method with U-Th measurements or with other dating techniques, as in our study. The possibility of He accumulation by diffusion from thermogenic natural gas deposits cannot be entirely excluded in our dataset, but it is unlikely given the low concentrations of radiogenic He ($<3\times10^{-8}$ ccSTP g^{-1}), and its absence from depths <250 m bgl may be explained by high sedimentation rates at the geologically young Bengal basin relative to He diffusion rates. Dowling et al. [2003] report radiogenic He values based on He and Ne measurements, and estimate ages of groundwater from ~100–240 m depth to be several hundred to over 1,000 years, assuming a radiogenic He accumulation rate 8-fold higher than in our study. However, if radiogenic He values of

Dowling et al. [2003] are plotted versus the $^{14}C_{DIC}$ data reported for the same set of wells by Aggarwal et al. [2000], and the samples affected by He diffusion from greater depths are excluded, the result is a correlation between the radiogenic He values and ^{14}C ages of 4.7×10^{-12} ccSTP g^{-1}_{GW} yr^{-1}. This is closer to the radiogenic He accumulation rate reported in the present study, suggesting that the rate used by Dowling et al. [2003] may have been overestimated and that the resulting ages were underestimated.

4.4. Perspectives on Late Pleistocene and Holocene climate from groundwater tracers

4.4.1. Stable isotopes ($^{2}H/^{1}H$, $^{18}O/^{16}O$, and $^{13}C/^{12}C$)—If the intermediate and deep aquifers were recharged ~10 kyr BP, groundwater could contain evidence of climate change during the Pleistocene to Holocene transition. Stable isotopes appear to have recorded some of these changes and, thus, lend further support to the dating method. Changing conditions toward a wetter climate can help explain why $\delta^{13}C$ in DIC and stable isotope ratios in the water molecule ($^{2}H/^{1}H$ and $^{18}O/^{16}O$) co-vary systematically and coherently toward lower values between 11 and 9,000 ^{14}C yr BP (Figs. 11 and S1).

The progressively lower $\delta^{2}H$ and $\delta^{18}O$ values by approximately 2‰ between 11 and 9,000 ^{14}C yr BP (Fig. 11a) suggest that the summer monsoon intensified over this time period, with a similar shift noted in dated groundwater archives from Bangladesh by Aggarwal et al. [2004]. A stronger monsoon would bring more isotopically depleted rains both due to larger amounts of precipitations [Dansgaard, [1964] and longer cyclone pathways, as seen in the province of Meghalaya, NE India today [Breitenbach et al., 2010]. The Bay of Bengal seawater was also more diluted at the onset of the Holocene by the influx of additional fresh water from global glacial melt and the stronger river flows in the Ganges-Brahmaputra-Meghna delta, resulting in more isotopically depleted rain being produced over the Bay of Bengal. Lowering of $\delta^{18}O$ values by 1–3‰ ca. 12–8 kyr BP has been related to a more intense and wetter SE Asian summer monsoon in a number of studies performed on foraminifera records or cave stalactites [Prins and Postma, 2000; Partin et al., 2007; Rashid et al., 2011], thus dated groundwater from the deep wells of Araihazar adds resolution to an otherwise small pool of groundwater stable isotopic archives [Aggarwal et al., 2000; Aggarwal et al., 2004; Majumder et al., 2011]. A similar pattern towards a ~2‰ lower $\delta^{18}O$ in groundwater is noted ca. 12–10 kyr BP for the uncorrected ^{14}C ages by Hoque and Burgess [2012], but the authors argue that a ^{13}C correction is necessary to account for the effects of carbonate dissolution on ^{14}C ages, after which the shift is no longer visible.

Climate change at the onset of the Holocene also helps explain the observed co-variations in $^{13}C/^{12}C$ and $^{14}C/^{12}C$ values in DIC without the need to invoke carbonate dissolution and apply ^{13}C correction to the radiocarbon ages. A possible explanation for the observed shift towards lower $^{13}C/^{12}C$ values in the DIC is a shift in vegetation cover as the summer South Asian monsoon intensified. Under a wetter regional climate regime, the C4-type grassy vegetation would give way to the C3-type vegetation, such as bushes, forests, and mangroves that produce organic carbon (OC) with more negative $\delta^{13}C$ values. The resulting deposition of sedimentary OC with a lower $\delta^{13}C$, as reported by Sarkar et al. [2009] for ~8 kyr old early Holocene sediment sitting atop the Last Glacial Maximum paleosol, would produce lower $\delta^{13}C$ in the DIC. A switch towards lower $\delta^{13}C$ values between 14–8 ^{14}C kyr BP is

also reported in bulk sediment organics of marine cores from the Bay of Bengal affected by continental OC inputs [Galy et al., 2008].

As the Holocene progressed, a slow return to slightly drier climate conditions and vegetation adapted to aridity was inferred from ^{13}C in sedimentary OC by Sarkar et al. [2009]. This trend is also noticeable in our data from shallow low-As groundwater where, excluding the three samples with deeper groundwater characteristics, $\delta^{13}C$ of DIC increases in tandem with increasing FM ^{14}C (Fig. 8). A similar temporal trend is also observed for $\delta^{18}O$ or $\delta^{2}H$, although it is somewhat distorted by the evaporative enrichment noted in several samples. In general, the trend toward more positive values in the shallow aquifer is less defined and more gradual over the course of the Holocene in comparison to the rapid decline of stable isotope ratios in the deep samples between 11 and 9,000 ^{14}C yr BP. Such a contrast argues for a rapid climate change with a leap in monsoon intensity at the onset of the Holocene, followed by a gradually increasing aridity since then.

Finally, recharge of the intermediate and deep aquifers by precipitation subject to little or no evaporation, as supported by stable isotopes of water ($\delta^{2}H$ and $\delta^{18}O$, Fig. 7), suggests that the groundwater recharge/vertical flow may have been faster at the time of transition between the Late Pleistocene and the Early Holocene. This observation argues for the existence of higher gradients at the onset of the Holocene and also suggests that many near-surface clay layers may have been eroded away by incised rivers, thus preventing the surface geology from holding as many ponds of water as today.

4.4.2. Noble gas temperatures—Noble gas temperatures (NGTs) calculated from the noble gas models reflect groundwater temperatures at the water table at the time of recharge. The NGT data from the intermediate and deep aquifer, as well as the oldest shallow aquifer sample (A7), suggest variations of recharge temperatures on the order of 3.5 °C (Fig. 5ab). Considering the uncertainty of the ages, and that these samples fall at the transition from the LGM to the Holocene, these variations suggest that some of the samples capture the colder, pre-Holocene period. In comparison, a ~3 °C lower sea surface T during the LGM is reported in the Bay of Bengal [Sarma et al., 2006; Rashid et al., 2011], which could translate into similar or larger T variations observed on land.

In the shallow low-As aquifer, except for one outlier sample with a low NGT and a fairly young age, the recharge temperatures appear to have remained more stable throughout the Holocene. Ranging from 23.6 to 25.9 °C, these temperatures are slightly lower than the current temperatures of 25.4 to 26.8 °C observed in the shallow aquifers near the water table. A possible explanation might be that the land use changes accompanying intensive agriculture in the recent decades have elevated ground and, therefore, water table temperatures compared to their historical Holocene levels due to the replacement of forests by fields [Stute and Sonntag, 1992].

A source of error in the NGT estimates might have been introduced by the uncertainty of the recharge area elevation. The model assumes recharge altitude to be at sea level, which may not be the case, especially for the samples from >90 m depth with long residence times and potentially longer flowpaths. The nearest highlands of the Tripura Hills, approximately 100

km east of our field site, as well as virtually all of the hilly areas within a 100–150 km distance, lie at elevations of <200 m above sea level (ASL). However, NGT overestimates of 0.8–0.9 °C, as determined from additional runs of the model assuming recharge at 200 m ASL, would be practically compensated for by the lower temperatures at that elevation due to the tropospheric lapse rate. Thus, the error introduced by the uncertainty of the recharge area elevation is minimal.

4.5 Basin-wide context of groundwater ages

Because the wells analyzed in the present study are all clustered within a 25 km^2 area, it is useful to place the observations in the regional context provided by other groundwater DIC ^{14}C measurements in the Bengal Basin. Except for very few samples, some of which might be impacted by shallow groundwater leaks or seawater mixing [Aggarwal et al., 2000; BGS/DPHE, 2001], most groundwater ^{14}C ages calculated in a way analogous to our C_1 ^{14}C age from depths >90 m are ~10,000 yr BP and similar to those found in our study [Aggarwal et al., 2000; BGS/DPHE, 2001; Hoque and Burgess, 2012]. A recent review compiled available ^{14}C ages by assuming that no dissolution of soil carbonates occurs within the vadose zone but correcting for the dissolution of radiocarbon-free carbonate along the groundwater flowpath by using the sample pH [Fendorf et al., 2010]. This analysis also placed an upper limit on ^{14}C ages in the Basin at depths >90 m bgl to ~10 kyr or older.

There are reports of groundwater $^{14}C_{DIC}$ ages as high as >20,000 yr BP [Aggarwal et al., 2000; BGS/DPHE, 2001; Majumder et al., 2011; Hoque and Burgess, 2012], but some younger ^{14}C ages have also been reported for deep wells along the eastern edges of the Bengal Basin [Majumder et al., 2011; Hoque and Burgess, 2012]. From these observations, Majumder et al. [2011] and Hoque and Burgess [2012] inferred the existence of flowpaths in the deep aquifer originating from the basin edges. The data from Araihazar do not support or reject this proposed pattern, but do indicate that the low-As aquifers are vertically stratified with respect to both the groundwater chemistry and flow, which was also observed to some extent by Hoque and Burgess [2012]. Whereas the shallow low-As aquifer is impacted by flows from the high-As aquifer, the intermediate to some extent, and in particular the deep aquifer, appear vertically isolated from the shallow aquifer, and if any significant flow occurs at this depth (>90 m bgl), it is probably predominantly lateral.

4.6. Implications for the sustainability of low-As aquifers

The new data from Araihazar show that As concentrations remain low in some of the shallow wells with the highest ^{3}H and ^{14}C concentrations (Fig. 3). This could be explained by As sorption onto the aquifer sands and the resulting transport retardation relative to groundwater containing ^{3}H [Stollenwerk et al., 2007; Radloff et al., 2011]. Alternatively, these areas of pronounced vertical recharge may coincide with areas where the overlying shallowest aquifer is well flushed by rapid recharge, and thus contains less As [Stute et al., 2007; Aziz et al., 2008; van Geen et al., 2008; Shamsudduha et al., 2015].

Conversely, the presence of modestly elevated dissolved As within the three shallow wells with 11–29 μg/L As (Table 1) does not appear related to recent recharge from the surface. Tritium is undetectable in two of the wells, while in the third it was detected in 2006 (0.27

TU), but fell below detection in 2011 when 29 μg/L As was measured. Elevated As in these shallow wells might instead be related to the fact that they were installed in greyish colored sand (Table 1). Thus, it appears that targeting orange sands at shallow and intermediate depths, accompanied by regular groundwater monitoring [van Geen et al., 2007], might still provide an affordable option in the short term for installing low-As wells in our study area.

In the long term, however, pumping from deep aquifers (>150 m bgl) is likely to increase as more drinking water wells and some irrigation wells switch to this source of low-As drinking water. The implications of continued or increased deep pumping on the viability of these low-As aquifers are explored in the light of three recharge scenarios for the deep aquifer corresponding to the Pleistocene to Holocene transition:

Under the first scenario, Pleistocene groundwater was trapped in the intermediate and deep aquifers (>90 m bgl) as the sea level rose at the onset of the Holocene (12–8 kyr BP), the strength of the summer monsoon intensified [Prins and Postma, 2000], and the young, Holocene sediment rapidly accumulated (11–6 kyr BP) [Goodbred and Kuehl, 2000a; Sarkar et al., 2009], reducing the horizontal flow gradients to a minimum. In this case, minimal recharge effectively occurred since the onset of the Holocene, therefore the flow regime would radically change with increased pumping from the deep aquifer, which has already created a cone of depression of 40–60 m around Dhaka that extends to the Jamuna (Brahmaputra), Padma (Ganges) and Meghna rivers [Hoque et al., 2007]. In Araihazar, located on the outskirts of this cone of depression, the average yearly vertical recharge to depths >150 m bgl has been recently estimated at 0.2 m/yr of Darcy flux.

Under the second scenario, groundwater flowed and continues to flow slowly from the basin edges, somewhat akin to the flow conceptualized by Michael and Voss [2009b], Majumder et al. [2011], and Hoque and Burgess [2012]. Assuming the nearest basin edge to be in the Tripura Hills, ~100 km due east, a constant advective velocity of ~10 m/yr would satisfy the observed groundwater ^{14}C age of ~10,000 years. Assuming a porosity of 0.3 and a representative horizontal hydraulic conductivity of 5×10^{-4} m/s from the basin-scale hydrological models of Michael and Voss [2008], such a flow velocity would require a horizontal hydraulic gradient in the deep aquifer of 2×10^{-4} or 0.2 m km^{-1}. This hydraulic gradient falls in the mid-range between the gradients estimated by BGS/DPHE [2001] to be 1 m km^{-1} in the north, and 0.01 m km^{-1} in the south of Bangladesh. The horizontal gradients induced by active pumping are larger and can significantly alter the flow regime in the future, especially at locations where cones of depression have developed. At the location of our study, 20–30 km east of the center of Dhaka cone of depression, lateral hydraulic gradients at depths >150 m bgl have recently ranged from 2×10^{-4} in the early dry season to 4×10^{-4} in the early.

The second scenario, i.e. that of the steady-state lateral flow from the basin edges, provides an upper limit on the amount of steady-state horizontal flow to the deep aquifer during the Mid-to-Late Holocene. Under non-steady-state conditions, however, it approaches the first scenario of the trapped Late Pleistocene-Early Holocene groundwater. For example, if groundwater found at depth >90 m bgl had recharged along much steeper horizontal and vertical gradients at the onset of the Holocene, the subsequent recharge rates during the Mid-

to-Late Holocene would have been much lower, allowing little flow to the aquifer until the recent deep pumping induced higher gradients and recharge rates again.

The third scenario reflects slow vertical recharge from the shallowest, high-As aquifer. A simple case of the uniform and constant vertical recharge would require an estimated advective velocity of ~2 cm/yr for the groundwater to reach a depth of 200 m bgl in 10,000 years. Assuming a porosity of 0.3, the recharge rate (Darcy velocity) would be 0.6 cm/yr, a reasonable value of vertical recharge (<1% of total precipitation) in a region that receives ~2 m/yr of precipitation [Harvey et al., 2006], and falling within the range of vertical leakage rates estimated for Araihazar by Zheng et al. [2005]. It is unlikely, however, that a long term, steady-state vertical recharge operates in the deep aquifer of Araihazar because of the observed stratification between the shallow aquifer, where various groundwater ages and chemical compositions are found, and the intermediate/deep aquifers that have a more uniform isotopic and chemical signature. It is also unlikely under natural conditions that downward flow would occur in the low-lying areas, as they would normally be the discharge areas of the longer, regional flowpaths. Vertical leakage, however, is induced locally at present by the deep pumping for industrial and/or agricultural purposes (0.2–0.6 m/yr) in the densely pumped areas [Harvey et al., 2002; Zheng et al., 2005; Michael and Voss, 2008]. Recent estimates of 0.2 m/yr of vertical (Darcy) recharge to depths >150 m bgl in Araihazar, based on the modeling of monitored water levels, are already one to two orders of magnitude higher than the long-term, uniform downward recharge estimated above from groundwater ages.

Whichever scenario is correct, vertical anisotropy appears to be have been sufficient to maintain a pronounced age contrast between the shallow and deeper aquifers in Araihazar and elsewhere in the Basin [Michael and Voss, 2009b; Hoque and Burgess, 2012]. However, the steady increase in hydraulic head differences between the shallow and intermediate aquifers, currently as large as 6.7 m at the location of monitoring well C5 (Fig. 2), indicate a growing potential for more rapid recharge of the deeper aquifers that could shorten the residence time of deep groundwater. As far as the future As status of the deep aquifer is concerned, the question is whether this new recharge will be mainly vertical, putting the system at risk of contamination by shallow groundwater, or whether the lateral recharge from major rivers and/or mountain ranges might also play a role. If the growing, localized cones of depression [Hoque et al., 2007] are far from or poorly connected to the lateral sources of recharge, a significant amount of vertical leakage of groundwater from the shallowest aquifer that contains high As and high DOC concentrations seems inevitable. Despite the protection afforded by adsorption onto the Pleistocene sediment [Stollenwerk et al., 2007; Radloff et al., 2011], preferential pathways likely exist that can speed up the vertical migration of As and DOC. On the other hand, if recharge from the basin edges to deeper aquifers occurs at present time, faster recharge from the highlands might be able to offset some of the pumping withdrawals and protect the deep aquifer to a certain degree from vertical intrusion of shallow groundwater. Lastly, if the deeper aquifers receive enhanced recharge from the major rivers flowing through the basin, as it may already be the case near the Meghna River in Araihazar, the effect such a scenario would have on its As status will depend on the type of sediment through which the river water flows on its way to the deep aquifer [Berg et al., 2008; van Geen et al., 2013].

A number of recent studies have raised concerns about the sustainability of the deep aquifer over the long term, especially if the irrigation pumping were to switch to the deep aquifer [Michael and Voss, 2008; Burgess et al., 2010; Mukherjee et al., 2011; Radloff et al., 2011]. Our data from Araihazar upazilla show that although recent recharge was found in the shallow and intermediate-depth low-As aquifers, no widespread intrusion of As has occurred at any depth of the low-As aquifers in the studied region. The finding is consistent with the recent study by Ravenscroft et al. [2013], which also offered a new ethical perspective by arguing that the benefits of limiting As exposure via drinking water and preserving crop yields outweigh the potential harm from contaminating the deep aquifer. Pumping of the deep aquifer for both the drinking water and irrigation may not be sustainable indefinitely, but may still be the best option until other ways to provide low-As drinking water are found.

5. Conclusions

This study identified two distinct zones within the 35–240 m bgl range for low-As aquifers across a 25 km^2 area of Bangladesh on the basis of a broad suite of groundwater tracers. At depths <90 m bgl, bomb ^3H and bomb ^{14}C indicate the presence of groundwater recharged <60 years ago and sourced in part from evaporated surface water, as evidenced by the stable isotope ratios. Groundwater chemistry at this depth is quite variable, and radiocarbon ages in DIC range from modern to ~10 kyr, indicating various degrees of mixing between older groundwater and recent recharge. High concentrations of ^3H and ^{14}C are not correlated with the presence or absence of clay in the well lithologs, nor do these samples bear evidence of As intrusion from the shallower depths.

The intermediate (90–150 m bgl) and deep aquifers (>150 m bgl) hold groundwater of uniform ^{14}C ages clustered at ~10 kyr BP, with only five of the 22 samples containing detectable ^3H (<0.3 TU, all five at intermediate depths <150 m bgl). A uniform groundwater chemical signature of low Na, low DIC and high Si is observed in intermediate and deep aquifers, and water stable isotopes indicate recharge with unevaporated rainwater. The radiocarbon ages from Araihazar are consistent with the accumulation of radiogenic ^4He calculated independently from noble gas measurements (He, Ne, Ar, Kr, and Xe). Systematic relationships between the intermediate and deep groundwater $^{13}C/^{12}C$, $^2H/^1H$, $^{18}O/^{16}O$, and radiocarbon, as well as variability in noble gas temperatures, suggest changes in monsoon intensity and shifts in dominance between the C4 and C3 vegetation at the onset of the Holocene.

If the deep aquifer (>150 m bgl) at this central location of the Bengal Basin was last substantially recharged ~10 kyr ago, concerns about its sustainable usage arise as the aquifer exploitation continues to grow and likely shortens the residence time of groundwater. The current stratification of groundwater ages and geochemical properties between the shallow, intermediate and deep low-As aquifers argues for a very slow deep aquifer recharge that is vertically isolated from the shallowest, high-arsenic aquifer. The aquifer response to increased pumping in the future, and its As status, will depend on whether shorter, vertical flowpaths are induced from the high-As aquifer or the longer flowpaths from basin edges can substantially recharge the aquifer at depth.

Supplementary Material

Refer to Web version on PubMed Central for supplementary material.

Acknowledgments

Data plotted in the Figures 6, 9, and 11 are available in Supporting Information Table S1. Our work in Araihazar, Bangladesh was supported primarily by NIEHS Superfund Research Program grant P42 ES010349. This is Lamont-Doherty Earth Observatory contribution number xxxx. I thank S. Shahud, L. Baker, R. Friedrich, and R. Newton for data acquisition help, as well as B. C. Bostick, P. S. K. Knappet, H. Michael, and C. F. Harvey for useful comments.

References

Aeschbach-Hertig W, Peeters F, Beyerle U, Kipfer R. Interpretation of dissolved atmospheric noble gases in natural waters. Water Resources Research. 1999; 35(9):2779–2792.

Aggarwal, PK., Basu, AR., Poreda, RJ., Kulkarni, KM., Froehlich, K., Tarafdar, SA., Ali, M., Ahmed, N., Hussain, A., Rahman, M., Ahmed, SR. IAEA-TC Project Report (BGD/8/016). International Atomic Energy Agency; Vienna: 2000. Isotope hydrology of groundwater in Bangladesh: Implications for characterization and mitigation of arsenic in groundwater.

Aggarwal PK, Fröhlich K, Kulkarni KM, Gourcy LL. Stable isotope evidence for moisture sources in the asian summer monsoon under present and past climate regimes. Geophysical Research Letters. 2004; 31(8):L08203.

Ahmed MF, Ahuja S, Alauddin M, Hug SJ, Lloyd JR, Pfaff A, Pichler T, Saltikov C, Stute M, van Geen A. Epidemiology - Ensuring safe drinking water in Bangladesh. Science. 2006; 314(5806): 1687–1688. [PubMed: 17170279]

Ali, M. Review of drilling and tubewell technology for groundwater irrigation. In: Rhaman, AA., Ravenscroft, P., editors. Groundwater Resources and Development in Bangladesh. The University Press Limited; Bangladesh: 2003. p. 197-219.

Aravena R, Wassenaar LI, Plummer LN. Estimating C-14 groundwater ages in a methanogenic aquifer. Water Resources Research. 1995; 31(9):2307–2317.

Argos M, Kalra T, Rathouz PJ, Chen Y, Pierce B, Parvez F, Islam T, Ahmed A, Rakibuz-Zaman M, Hasan R, Sarwar G, Slavkovich V, van Geen A, Graziano J, Ahsan H. Arsenic exposure from drinking water, and all-cause and chronic-disease mortalities in Bangladesh (HEALS): a prospective cohort study. Lancet. 2010; 376(9737):252–258. [PubMed: 20646756]

Aziz Z, van Geen A, Stute M, Versteeg R, Horneman A, Zheng Y, Goodbred S, Steckler M, Weinman B, Gavrieli I, Hoque MA, Shamsudduha M, Ahmed KM. Impact of local recharge on arsenic concentrations in shallow aquifers inferred from the electromagnetic conductivity of soils in Araihazar, Bangladesh. Water Resources Research. 2008; 44(7)

Bayer, R., Schlosser, P., Boenisch, G., Rupp, H., Zaucker, F., Zimmek, G. Sitzungsberichte (5). Heidelberger Akademie der Wissenschaften, Mathematisch-naturwissenschaftliche Klasse, Jahrgang; Heidelberg, Germany: 1989. Performance and blank components of a mass spectrometric system for routine measurement of helium isotopes and tritium by the He-3 ingrowth method; p. 241-279.

Berg M, Trang PTK, Stengel C, Buschmann J, Viet PH, Van Dan N, Giger W, Stueben D. Hydrological and sedimentary controls leading to arsenic contamination of groundwater in the Hanoi area, Vietnam: The impact of iron-arsenic ratios, peat, river bank deposits, and excessive groundwater abstraction. Chemical Geology. 2008; 249(1–2):91–112.

BGS/DPHE. Arsenic contamination of groundwater in Bangladesh. In: Kinniburgh, DG., Smedley, PL., editors. BGS technical Report WC/00/19. British Geological Survey; Keyworth, UK: 2001.

Breitenbach SFM, Adkins JF, Meyer H, Marwan N, Kumar KK, Haug GH. Strong influence of water vapor source dynamics on stable isotopes in precipitation observed in Southern Meghalaya, NE India. Earth and Planetary Science Letters. 2010; 292(1–2):212–220.

Burgess WG, Hoque MA, Michael HA, Voss CI, Breit GN, Ahmed KM. Vulnerability of deep groundwater in the Bengal Aquifer System to contamination by arsenic. Nature Geoscience. 2010; 3(2):83–87.

Chabaux F, Blaes E, Granet M, Roupert RD, Stille P. Determination of transfer time for sediments in alluvial plains using U-238-U-234-Th-230 disequilibria: The case of the Ganges river system. C R Geosci. 2012; 344(11–12):688–703.

Cheng Z, Zheng Y, Mortlock R, van Geen A. Rapid multi-element analysis of groundwater by high-resolution inductively coupled plasma mass spectrometry. Analytical and Bioanalytical Chemistry. 2004; 379(3)

Choudhury I, Ahmed KM, Hasan M, Mozumder MRH, Knappett PSK, Ellis T, van Geen A. Evidence for Elevated Levels of Arsenic in Public Wells of Bangladesh Due To Improper Installation. Groundwater. 2016; doi: 10.1111/gwat.12417

Chowdhury MI, Alam MN, Hazari SKS. Distribution of radionuclides in the river sediments and coastal soils of Chittagong, Bangladesh and evaluation of the radiation hazard. Appl Radiat Isot. 1999; 51(6):747–755.

Clarke WB, Jenkins WJ, Top Z. Determination of tritium by mass-spectrometric measurement of He-3. International Journal of Applied Radiation and Isotopes. 1976; 27(9):515–522.

Craig H. Isotopic variations in meteoric waters. Science. 1961; 133(346):1702–1703. [PubMed: 17814749]

Craig H, Lupton JE. Primordial neon, helium, and hydrogen in oceanic basalts. Earth and Planetary Science Letters. 1976; 31(3):369–385.

Dansgaard W. Stable isotopes in precipitation. Tellus. 1964; 16(4):436–468.

Dhar RK, Zheng Y, Stute M, van Geen A, Cheng Z, Shanewaz M, Shamsudduha M, Hoque MA, Rahman MW, Ahmed KM. Temporal variability of groundwater chemistry in shallow and deep aquifers of Araihazar, Bangladesh. Journal of Contaminant Hydrology. 2008; 99(1–4):97–111. [PubMed: 18467001]

Dowling CB, Poreda RJ, Basu AR. The groundwater geochemistry of the Bengal Basin: Weathering, chemsorption, and trace metal flux to the oceans. Geochimica Et Cosmochimica Acta. 2003; 67(12):2117–2136.

DPHE/JICA. Report on Situation Analysis of Arsenic Mitigation, 2009. Dept of Public Health Engineering, Local Government Division, Government of Bangladesh and Japan International Cooperation Agency; 2010.

Eastoe CJ, Watts CJ, Ploughe M, Wright WE. Future use of tritium in mapping pre-bomb groundwater volumes. Groundwater. 2012; 50(1):87–93.

Elder KL, McNichol AP, Gagnon AR. Evaluating reproducibility of seawater, inorganic and organic carbon 14C results at the National Ocean Sciences AMS Facility (NOSAMS): Proceedings of the 16th International Radiocarbon Conference. Radiocarbon. 1997; 40:223–230.

Fendorf S, Michael HA, van Geen A. Spatial and Temporal Variations of Groundwater Arsenic in South and Southeast Asia. Science. 2010; 328(5982):1123–1127. [PubMed: 20508123]

Fontes JC, Garnier JM. Determination of the initial C-14 activity of the total dissolved carbon - review of the existing models and a new approach. Water Resources Research. 1979; 15(2):399–413.

Galy V, Francois L, France-Lanord C, Faure P, Kudrass H, Palhol F, Singh SK. C4 plants decline in the Himalayan basin since the Last Glacial Maximum. Quat Sci Rev. 2008; 27(13–14):1396–1409.

Goodbred SL, Kuehl SA. Enormous Ganges-Brahmaputra sediment discharge during strengthened early Holocene monsoon. Geology. 2000a; 28(12):1083–1086.

Goodbred SL, Kuehl SA. The significance of large sediment supply, active tectonism, and eustasy on margin sequence development: Late Quaternary stratigraphy and evolution of the Ganges-Brahmaputra delta. Sedimentary Geology. 2000b; 133(3–4):227–248.

Gran G. Determination of the equivalence point in potentiometric titrations. 2. Analyst. 1952; 77(920): 661–671.

Granet M, Chabaux F, Stille P, France-Lanord C, Pelt E. Time-scales of sedimentary transfer and weathering processes from U-series nuclides: Clues from the Himalayan rivers. Earth and Planetary Science Letters. 2007; 261(3–4):389–406.

Granet M, Chabaux F, Stille P, Dosseto A, France-Lanord C, Blaes E. U-series disequilibria in suspended river sediments and implication for sediment transfer time in alluvial plains: The case of the Himalayan rivers. Geochimica Et Cosmochimica Acta. 2010; 74(10):2851–2865.

Harvey CF, Ashfaque KN, Yu W, Badruzzaman ABM, Ali MA, Oates PM, Michael HA, Neumann RB, Beckie R, Islam S, Ahmed MF. Groundwater dynamics and arsenic contamination in Bangladesh. Chemical Geology. 2006; 228(1–3):112–136.

Harvey CF, Swartz CH, Badruzzaman ABM, Keon-Blute N, Yu W, Ali MA, Jay J, Beckie R, Niedan V, Brabander D, Oates PM, Ashfaque KN, Islam S, Hemond HF, Ahmed MF. Arsenic mobility and groundwater extraction in Bangladesh. Science. 2002; 298(5598):1602–1606. [PubMed: 12446905]

Hoque MA, Burgess WG. C-14 dating of deep groundwater in the Bengal Aquifer System, Bangladesh: Implications for aquifer anisotropy, recharge sources and sustainability. Journal of Hydrology. 2012; 444:209–220.

Hoque MA, Hoque MM, Ahmed KM. Declining groundwater level and aquifer dewatering in Dhaka metropolitan area, Bangladesh: causes and quantification. Hydrogeology Journal. 2007; 15(8): 1523–1534.

Horneman A, van Geen A, Kent DV, Mathe PE, Zheng Y, Dhar RK, O'Connell S, Hoque MA, Aziz Z, Shamsudduha M, Seddique AA, Ahmed KM. Decoupling of As and Fe release to Bangladesh groundwater under reducing conditions. Part 1: Evidence from sediment profiles. Geochimica Et Cosmochimica Acta. 2004; 68(17):3459–3473.

Ingerson, E., Pearson, FJJ. Recent Researches in the Fields of Hydrosphere, Atmosphere and Nuclear Geochemistry. Maruzen; Tokyo: 1964. Estimation of age and rate of motion of groundwater by the 14C-method; p. 263-283.

Ludin, AR., Weppernig, R., Boenisch, G., Schlosser, P. Lamont-Doherty Earth Observatory. Palisades; New York: 1998. Mass spectrometric measurement of helium isotopes and tritium, internal report.

Mailloux BJ, Trembath-Reichert E, Cheung J, Watson M, Stute M, Freyer GA, Ferguson AS, Ahmed KM, Alam MJ, Buchholz BA, Thomas J, Layton AC, Zheng Y, Bostick BC, van Geen A. Advection of surface-derived organic carbon fuels microbial reduction in Bangladesh groundwater. Proceedings of the National Academy of Sciences of the United States of America. 2013; 110(14): 5331–5335. [PubMed: 23487743]

Majumder RK, Halim MA, Saha BB, Ikawa R, Nakamura T, Kagabu M, Shimada J. Groundwater flow system in Bengal Delta, Bangladesh revealed by environmental isotopes. Environmental Earth Sciences. 2011; 64(5):1343–1352.

McArthur JM, Sikdar PK, Hoque MA, Ghosal U. Waste-water impacts on groundwater: Cl/Br ratios and implications for arsenic pollution of groundwater in the Bengal Basin and Red River Basin, Vietnam. Science of the Total Environment. 2012; 437:390–402. [PubMed: 22960402]

McArthur JM, Nath B, Banerjee DM, Purohit R, Grassineau N. Palaeosol Control on Groundwater Flow and Pollutant Distribution: The Example of Arsenic. Environmental Science & Technology. 2011; 45(4):1376–1383. [PubMed: 21268629]

McArthur JM, Banerjee DM, Sengupta S, Ravenscroft P, Klump S, Sarkar A, Disch B, Kipfer R. Migration of As, and H-3/(3) He ages, in groundwater from West Bengal: Implications for monitoring. Water Research. 2010; 44(14):4171–4185. [PubMed: 20542311]

McArthur JM, Ravenscroft P, Banerjee DM, Milsom J, Hudson-Edwards KA, Sengupta S, Bristow C, Sarkar A, Tonkin S, Purohit R. How paleosols influence groundwater flow and arsenic pollution: A model from the Bengal Basin and its worldwide implication. Water Resources Research. 2008; 44(11)

Michael HA, Voss CI. Evaluation of the sustainability of deep groundwater as an arsenic-safe resource in the Bengal Basin. Proceedings of the National Academy of Sciences of the United States of America. 2008; 105(25):8531–8536. [PubMed: 18562284]

Michael HA, Voss CI. Controls on groundwater flow in the Bengal Basin of India and Bangladesh: regional modeling analysis. Hydrogeology Journal. 2009a; 17(7):1561–1577.

Michael HA, Voss CI. Estimation of regional-scale groundwater flow properties in the Bengal Basin of India and Bangladesh. Hydrogeology Journal. 2009b; 17(6):1329–1346.

Mihajlov, I. PhD thesis. Department of Earth and Environmental Sciences, Columbia University; New York, NY: 2014. The vulnerability of low-arsenic aquifers in Bangladesh: a multi-scale geochemical and hydrologic approach.

Molla NI, Hossain SM, Basunia S, Miah RU, Rahman M, Sikder DH, Chowdhury MI. Elemental analysis in bed sediment samples of Karnafuli estuarine zone in the Bay of Bengal by instrumental neutron activation analysis. J Radioanal Nucl Chem. 1997; 216(2):213–215.

Mukherjee A, Fryar AE, Scanlon BR, Bhattacharya P, Bhattacharya A. Elevated arsenic in deeper groundwater of the western Bengal basin, India: Extent and controls from regional to local scale. Applied Geochemistry. 2011; 26(4):600–613.

Olsson, IU. The use of Oxalic acid as a Standard. In: Olsson, IU., editor. Radiocarbon Variations and Absolute Chronology, Nobel Symposium, 12th Proc. John Wiley & Sons; New York: 1970. p. 17

Partin JW, Cobb KM, Adkins JF, Clark B, Fernandez DP. Millennial-scale trends in west Pacific warm pool hydrology since the Last Glacial Maximum. Nature. 2007; 449(7161):452–U453. [PubMed: 17898765]

Peeters F, Beyerle U, Aeschbach-Hertig W, Holocher J, Brennwald MS, Kipfer R. Improving noble gas based paleoclimate reconstruction and groundwater dating using Ne-20/Ne-22 ratios. Geochimica Et Cosmochimica Acta. 2003; 67(4):587–600.

Plummer LN, Eggleston JR, Andreasen DC, Raffensperger JP, Hunt AG, Casile GC. Old groundwater in parts of the upper Patapsco aquifer, Atlantic Coastal Plain, Maryland, USA: evidence from radiocarbon, chlorine-36 and helium-4. Hydrogeology Journal. 2012; 20(7):1269–1294.

Prins MA, Postma G. Effects of climate, sea level, and tectonics unraveled for last deglaciation turbidite records of the Arabian Sea. Geology. 2000; 28(4):375–378.

Radloff KA, Zheng Y, Michael HA, Stute M, Bostick BC, Mihajlov I, Bounds M, Huq MR, Choudhury I, Rahman MW, Schlosser P, Ahmed KM, van Geen A. Arsenic migration to deep groundwater in Bangladesh influenced by adsorption and water demand. Nature Geoscience. 2011; 4(11):793–798.

Rashid H, England E, Thompson L, Polyak L. Late Glacial to Holocene Indian Summer Monsoon Variability Based upon Sediment Records Taken from the Bay of Bengal. Terr Atmos Ocean Sci. 2011; 22(2):215–228.

Ravenscroft P, McArthur JM. Mechanism of regional enrichment of groundwater by boron: the examples of Bangladesh and Michigan, USA. Applied Geochemistry. 2004; 19(9):1413–1430.

Ravenscroft, P., Brammer, H., Richards, KS. Arsenic pollution: a global synthesis. Wiley-Blackwell; Chichester, UK: 2009.

Ravenscroft P, McArthur JM, Hoque MA. Stable groundwater quality in deep aquifers of Southern Bangladesh: The case against sustainable abstraction. Science of the Total Environment. 2013; 454:627–638. [PubMed: 23584139]

Ravenscroft P, Kabir A, Hakim SAI, Ibrahim AKM, Ghosh SK, Rahman MS, Akter F, Sattar MA. Effectiveness of public rural waterpoints in Bangladesh with special reference to arsenic mitigation. Journal of Water, Sanitation and Hygiene for Development. 2014; 4(4):545–562. DOI: 10.2166/washdev.2014.038

Ravenscroft P, Burgess WG, Ahmed KM, Burren M, Perrin J. Arsenic in groundwater of the Bengal Basin, Bangladesh: Distribution, field relations, and hydrogeological setting. Hydrogeology Journal. 2005; 13(5–6):727–751.

Sarkar A, Sengupta S, McArthur JM, Ravenscroft P, Bera MK, Bhushan R, Samanta A, Agrawal S. Evolution of Ganges-Brahmaputra western delta plain: clues from sedimentology and carbon isotopes. Quat Sci Rev. 2009; 28(25–26):2564–2581.

Sarma NS, Pasha SG, Krishna MSR, Shirodkar PV, Yadava MG, Rao KM. Long-chain alkenone unsaturation index as sea surface temperature proxy in southwest Bay of Bengal. Curr Sci. 2006; 91(1):82–86.

Shamsudduha M, Taylor RG, Chandler RE. A generalized regression model of arsenic variations in the shallow groundwater of Bangladesh. Water Resources Research. 2015; 51:685–703. [PubMed: 27524841]

Smith AH, Lingas EO, Rahman M. Contamination of drinking-water by arsenic in Bangladesh: a public health emergency. Bulletin of the World Health Organization. 2000; 78(9):1093–1103. [PubMed: 11019458]

Stollenwerk KG, Breit GN, Welch AH, Yount JC, Whitney JW, Foster AL, Uddin MN, Majumder RK, Ahmed N. Arsenic attenuation by oxidized aquifer sediments in Bangladesh. Science of the Total Environment. 2007; 379(2–3):133–150. [PubMed: 17250876]

Stute M, Clark JF, Schlosser P, Broecker WS, Bonani G. A 30,000 yr Continental Paleotemperature Record Derived from Noble Gases Dissolved in Groundwater from the San Juan Basin, New Mexico. Quaternary Research. 1995; 43(2):209–220.

Stute, M., Sonntag, C. Isotopes of noble gases as tracers in environmental studies. IAEA; Vienna: 1992. Paleotemperatures derived from noble gases dissolved in groundwater and relation to soil temperature; p. 111-122.

Stute M, Zheng Y, Schlosser P, Horneman A, Dhar RK, Datta S, Hoque MA, Seddique AA, Shamsudduha M, Ahmed KM, van Geen A. Hydrological control of As concentrations in Bangladesh groundwater. Water Resources Research. 2007; 43(9)

Torgersen T. Controls on pore-fluid concentration of the He-4 and Rn-222 and the calculation of He-4/Rn-222 ages. J Geochem Explor. 1980; 13(1):57–75.

Torgersen T. Terrestrial helium degassing fluxes and the atmospheric helium budget: Implications with respect to the degassing processes of continental crust. Chemical Geology. 1989; 79(1):1–14.

Torgersen T, Clarke WB. Helium accumulation in groundwater, I: An evaluation of sources and the continental flux of crustal He-4 in the Great Artesian Basin, Australia. Geochimica Et Cosmochimica Acta. 1985; 49(5):1211–1218.

van Geen A, Cheng ZQ, Jia Q, Seddique AA, Rahman MW, Rahman MM, Ahmed KM. Monitoring 51 community wells in Araihazar, Bangladesh, for up to 5 years: Implications for arsenic mitigation. Journal of Environmental Science and Health Part A -Toxic/Hazardous Substances & Environmental Engineering. 2007; 42(12):1729–1740.

van Geen A, Zheng Y, Versteeg R, Stute M, Horneman A, Dhar R, Steckler M, Gelman A, Small C, Ahsan H, Graziano JH, Hussain I, Ahmed KM. Spatial variability of arsenic in 6000 tube wells in a 25 km(2) area of Bangladesh. Water Resources Research. 2003; 39(5)

van Geen A, Zheng Y, Goodbred S Jr, Horneman A, Aziz Z, Cheng Z, Stute M, Mailloux B, Weinman B, Hoque MA, Seddique AA, Hossain MS, Chowdhury SH, Ahmed KM. Flushing history as a hydrogeological control on the regional distribution of arsenic in shallow groundwater of the Bengal Basin. Environmental Science & Technology. 2008; 42(7):2283–2288. [PubMed: 18504954]

van Geen A, Bostick BC, Trang PTK, Lan VM, Mai N-N, Manh PD, Viet PH, Radloff K, Aziz Z, Mey JL, Stahl MO, Harvey CF, Oates P, Weinman B, Stengel C, Frei F, Kipfer R, Berg M. Retardation of arsenic transport through a Pleistocene aquifer. Nature. 2013; 501:204–207. [PubMed: 24025840]

van Geen A, Ahmed KM, Ahmed EB, Choudhury I, Mozumder MR, Bostick BC, Mailloux BJ. Inequitable allocation of deep community wells for reducing arsenic exposure in Bangladesh. Journal of Water, Sanitation and Hygiene for Development. 2015; doi: 10.2166/washdev.2015.115

Verhagen BT, Mazor E, Sellschop JPF. Radiocarbon and tritium evidence for direct rain recharge to ground waters in northern Kalahari. Nature. 1974; 249(5458):643–644.

Vogel, JC. Isotopes in Hydrology. International Atomic Energy Agency; Vienna: 1967. Investigation of groundwater flow with radiocarbon; p. 355-368.

Vogel, JC., Ehhalt, D. Radioisotopes in Hydrology. International Atomic Energy Agency; Vienna: 1963. The use of carbon isotopes in groundwater studies; p. 383-395.

Wasserman GA, Liu X, Parvez F, Ahsan H, Factor-Litvak P, van Geen A, Slavkovich V, Lolacono NJ, Cheng Z, Hussain I, Momotaj H, Graziano JH. Water arsenic exposure and children's intellectual function in Araihazar, Bangladesh. Environmental Health Perspectives. 2004; 112(13):1329–1333. [PubMed: 15345348]

Weiss W, Roether W. The rates of tritium input to the world oceans. Earth and Planetary Science Letters. 1980; 49(2):435–446.

Weiss, W., Bullacher, J., Roether, W. Behaviour of Tritium in the Environment, IAEA-SM-232118. International Atomic Energy Agency; Vienna: 1979. Evidence of pulsed discharges of tritium from nuclear energy installations in Central Europe precipitation; p. 17-30.

Zheng Y, Stute M, van Geen A, Gavrieli I, Dhar R, Simpson HJ, Schlosser P, Ahmed KM. Redox control of arsenic mobilization in Bangladesh groundwater. Applied Geochemistry. 2004; 19(2)

Zheng Y, van Geen A, Stute M, Dhar R, Mo Z, Cheng Z, Horneman A, Gavrieli I, Simpson HJ, Versteeg R, Steckler M, Grazioli-Venier A, Goodbred S, Shahnewaz M, Shamsudduha M, Hoque MA, Ahmed KM. Geochemical and hydrogeological contrasts between shallow and deeper aquifers in two villages of AraihazarBangladesh: Implications for deeper aquifers as drinking water sources. Geochimica Et Cosmochimica Acta. 2005; 69(22):5203–5218.

Key points

- Tritium is detected down to nearly 150 m depth in low-arsenic aquifers east of Dhaka, Bangladesh
- Noble gas and stable isotope measurements are used to validate ^{14}C dating of deep Bengal groundwater
- Low-arsenic aquifers at depths >90 m were predominantly recharged ~10 kyr ago at a time of rapidly changing climate

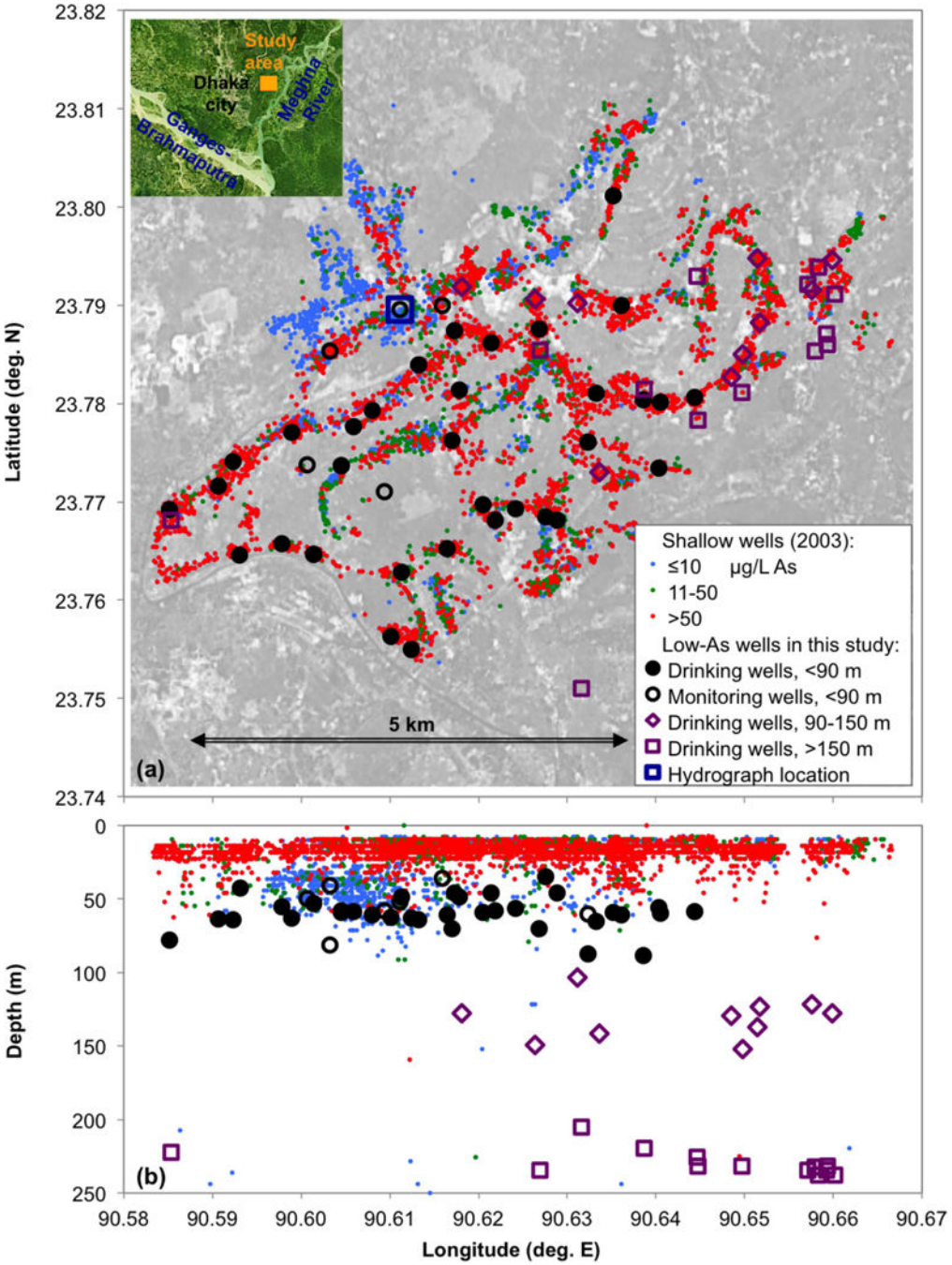

Figure 1.

(a) Map of the field area in Araihazar upazilla, Bangladesh, and (b) depth distribution of the wells. The low-arsenic wells discussed in this work are marked by large circles, diamonds, and squares. In this figure, and hereafter, the data are plotted as black circles for low-As groundwater from shallow depth (<90 m bgl), open purple diamonds for intermediate aquifer (90–150 m bgl), and open purple squares for deep groundwater (>150 m bgl). In this figure only, the distinction is also made between drinking (filled circles) and monitoring wells (open circles) installed within the shallow low-As aquifer; in subsequent figures, all

shallow samples are rendered as filled black circles. The small circles in the background show the distribution of surveyed private, mostly shallow tubewells [van Geen et al., 2003] and are color-coded for As concentrations. The orientation of Araihazar field area (red square) with respect to Dhaka, Bangladesh and the major rivers is indicated by the inset in map (a).

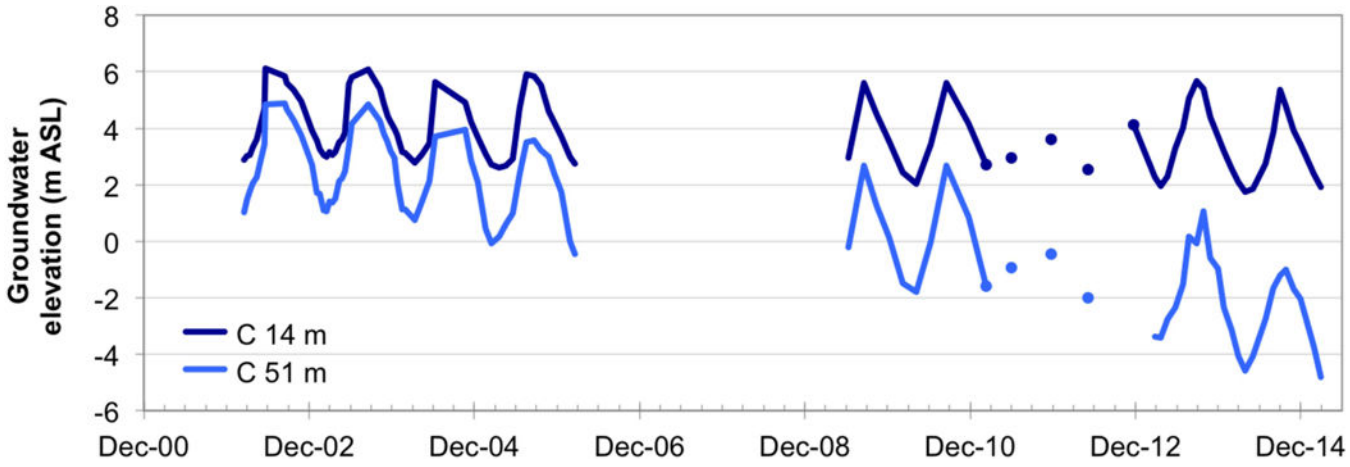

Figure 2.

Hydrographs of a very shallow, high-arsenic well (14 m bgl) and a shallow-depth, low-arsenic well (C5 in this study, 51 m bgl) at the location of multi-level nest C, designated by the large blue square in Fig. 1(a). Hydraulic head data since 2001 indicate a steadily declining water level of the deeper, low-As well, and thus an increasing downward vertical hydraulic gradient between the shallowest and the deepest wells at this site.

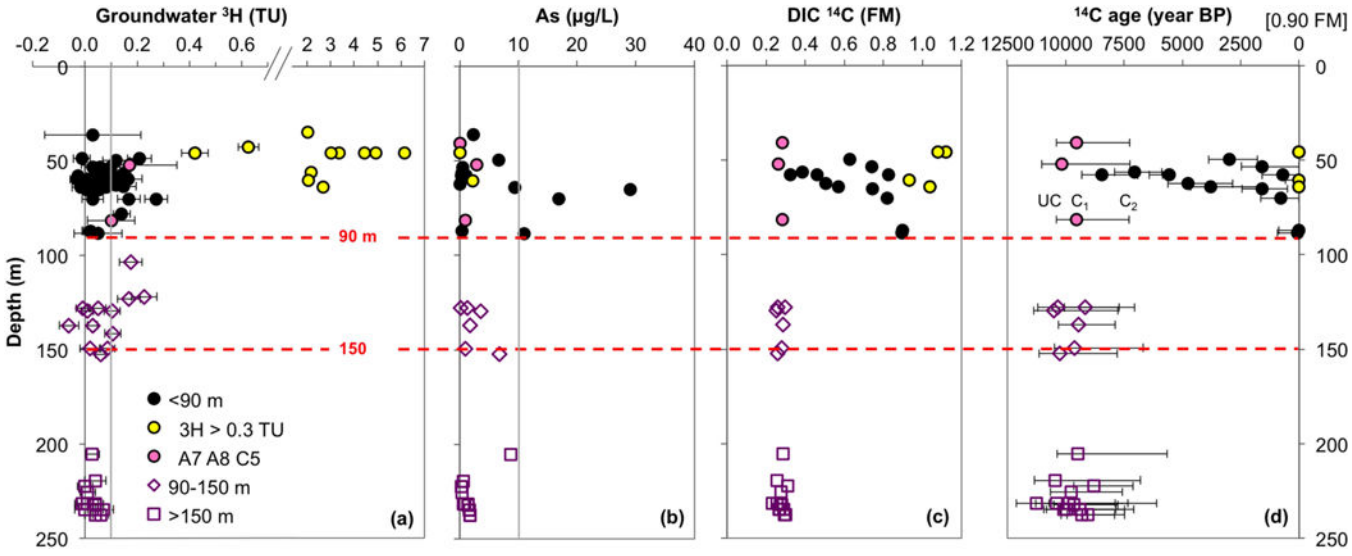

Figure 3.

Profiles of groundwater (a) ^{3}H with analytical error, (b) dissolved As, (c) ^{14}C in DIC, and (d) ^{14}C ages plotted against sample depth. All ^{3}H measurements, including several repeat measurements, are shown; for samples where ^{14}C was measured twice, $^{14}C_{DIC}$ and calculated ages plotted in this figure, and hereafter, are based on the ^{14}C values obtained in 2010. The grey line in (a) indicates 0.1 TU, the concentration above which all ^{3}H samples (except for two with a large analytical error) are conclusively detectable, whereas the grey line in (b) denotes the current World Health Organization limit of 10 µg/L As in safe drinking water. The symbols in (d) show C_1 ^{14}C age, a simple open system model that corrects for the initial $^{14}C_{DIC}$ at recharge of 0.90 FM. The error bars indicate “UC” (uncorrected) ^{14}C age as the maximum age, calculated directly from the measured ^{14}C values without any correction, and C_2 ^{14}C age as the minimum age, which contains an additional correction for the maximum contribution of radiocarbon-dead carbonate dissolution along the flowpath. In this figure, and hereafter, the pink fill in black circles indicates the shallow depth samples (A7, A8, and C5) with consistent deeper groundwater properties across various geochemical and age parameters, whereas the yellow fill in black circles denotes shallow aquifer groundwater with particularly elevated ^{3}H concentrations (>0.3 TU).

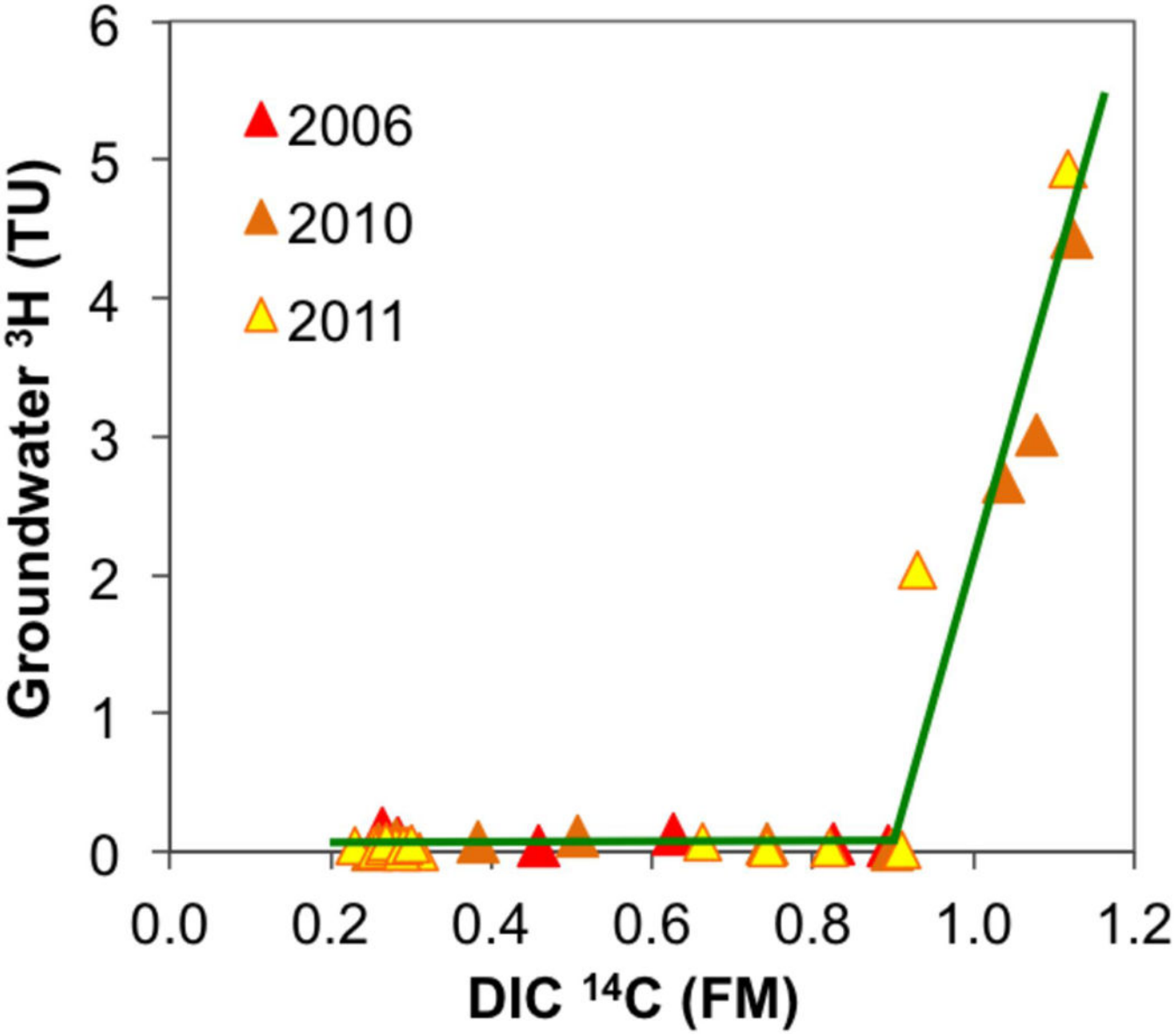

Figure 4.

Empirical relationship between groundwater ^{3}H and ^{14}C in DIC plotted for all available samples from the shallow, low-As aquifer (<90 m bgl) with concurrently measured groundwater ^{3}H and ^{14}C in DIC. The initial $^{14}C_{DIC}$ was determined to be 0.90 FM and used to correct for the vadose zone processes before the recharge closed off from the atmosphere in C_1 and C_2 ^{14}C age calculations.

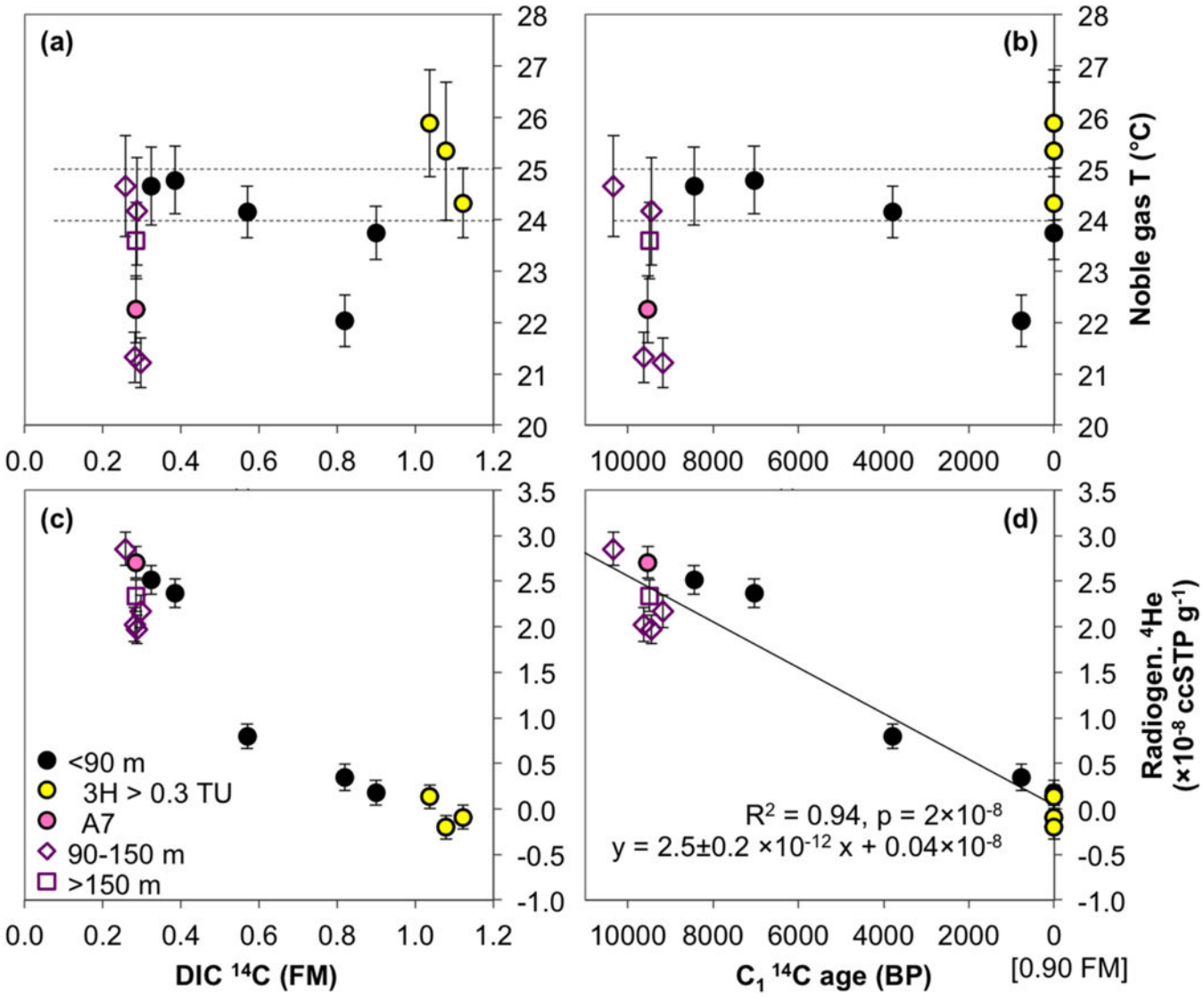

Figure 5.

Noble gas temperatures and radiogenic ("excess") He plotted against ^{14}C measured in DIC (a and c), and corrected C_1 ^{14}C ages (b and d). Noble gas temperatures, corresponding to temperatures at the time of recharge, and radiogenic He were estimated by Taf-1 model fit to the measured noble gas data. Only the samples where model converged are plotted. The errors indicated by vertical error bars combine the analytical error with model fit uncertainty. Only one sample per well is shown; where multiple noble gas measurements were made, those with the best noble gas model fit are displayed. Dashed lines in (a) and (b) mark the 95% confidence interval of the average noble gas temperatures of shallow samples, excluding the two outliers at approximately 22 °C. The trend linking radiogenic He to C_1 ^{14}C ages was calculated fo

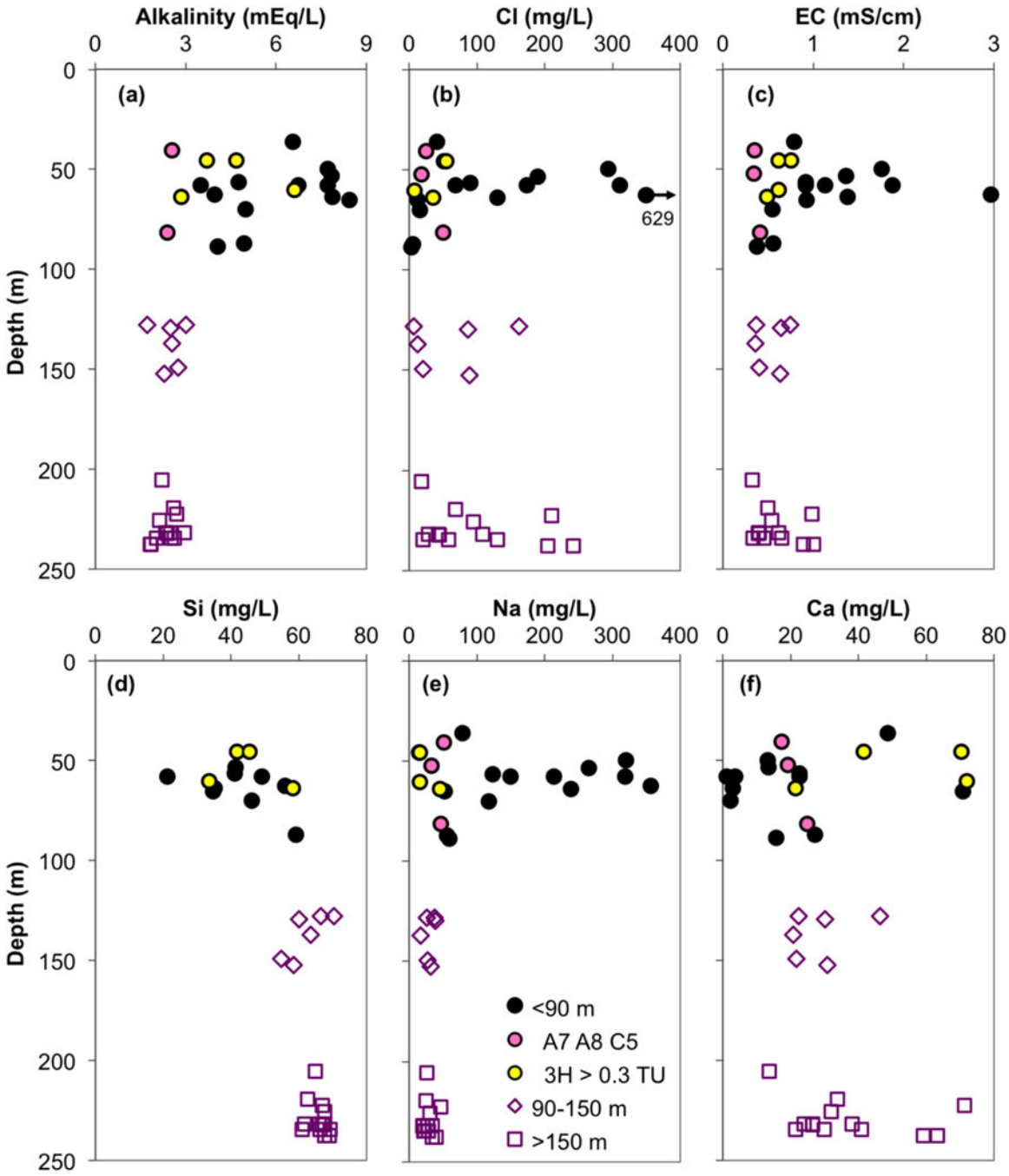

Figure 6.
Profiles of groundwater (a) alkalinity, (b) chloride, (c) electrical conductivity, (d) silicon, (e) sodium, and (f) calcium plotted against the sample depth.

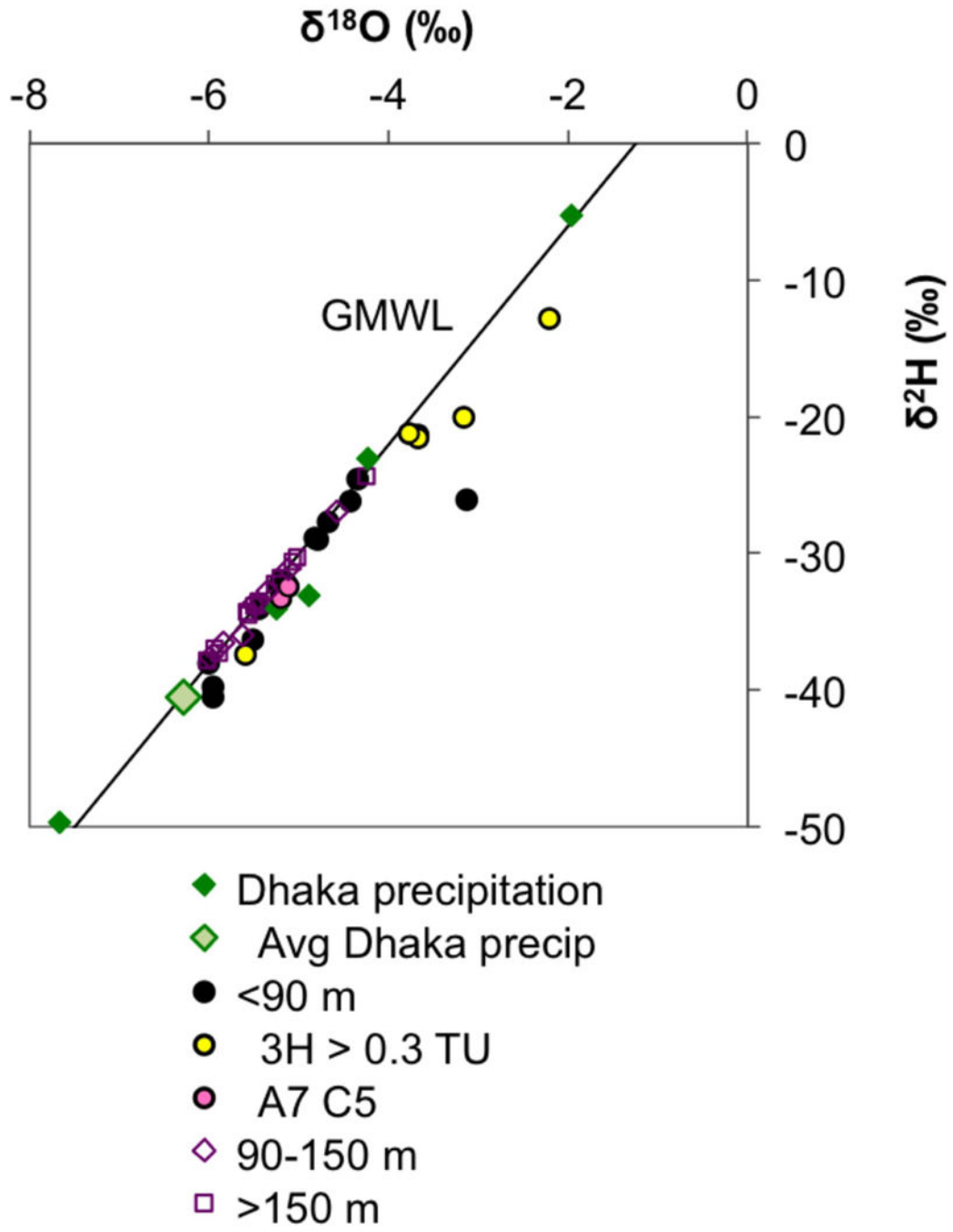

Figure 7.

Water stable isotopic (δ^2H and $\delta^{18}O$) composition of groundwater and its relationship to the global meteoric water line (GMWL) of Craig [1961]. For comparison, Dhaka precipitation and its average [Stute et al., 2007] are also displayed. Note that the high-^3H samples (yellow fill) plot mostly to the right of the GMWL.

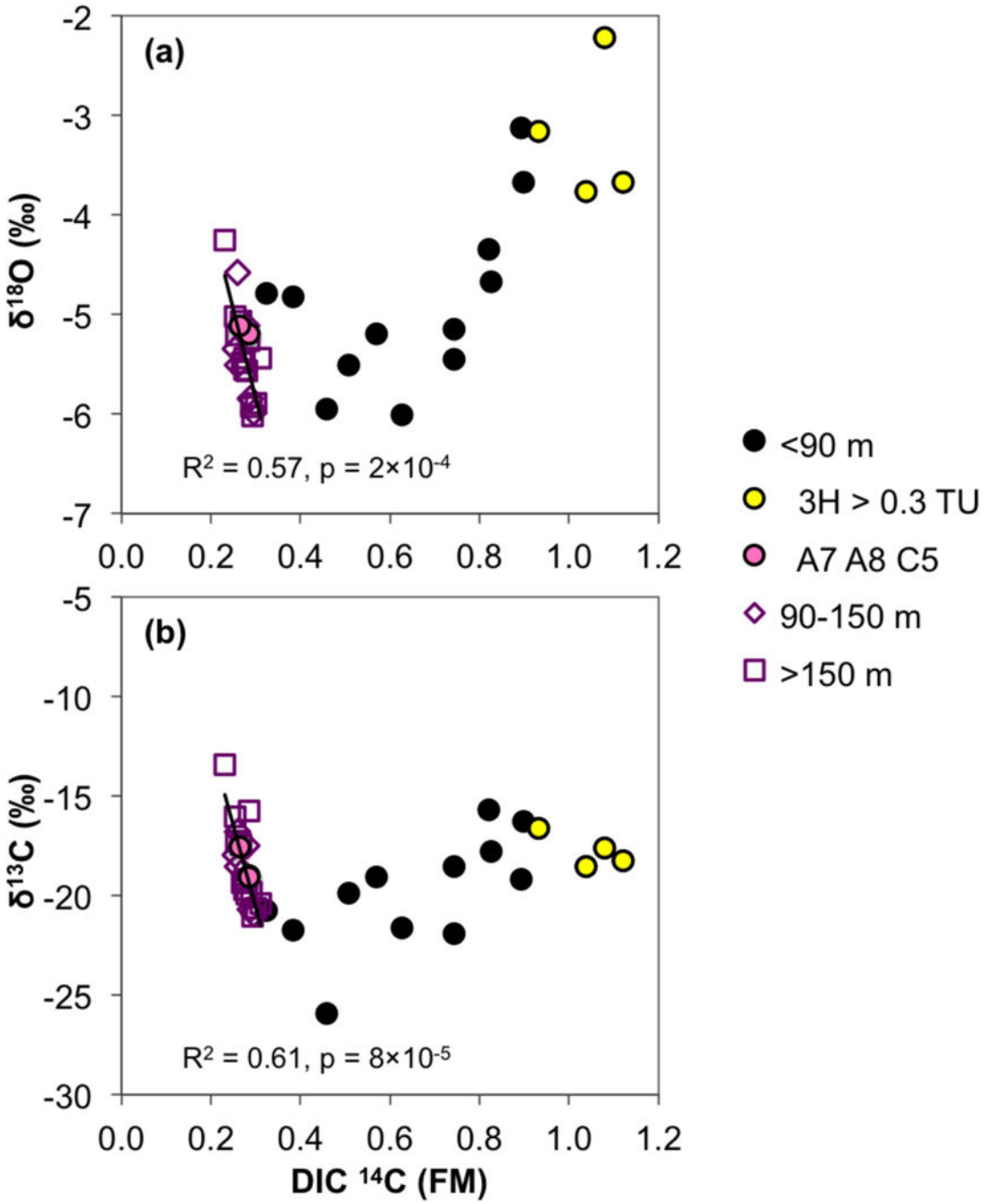

Figure 8.

The relationship of (a) water $\delta^{18}O$ and (b) DIC $\delta^{13}C$ with ^{14}C in DIC. The trendlines, R^2 and p values for pooled intermediate (90–150 m bgl) and deep aquifer (>150 m bgl) samples are indicated. A similar pattern to (a) is also observed for $\delta^{2}H$ (not shown, $R^2 = 0.60$ and $p = 1\times10^{-4}$).

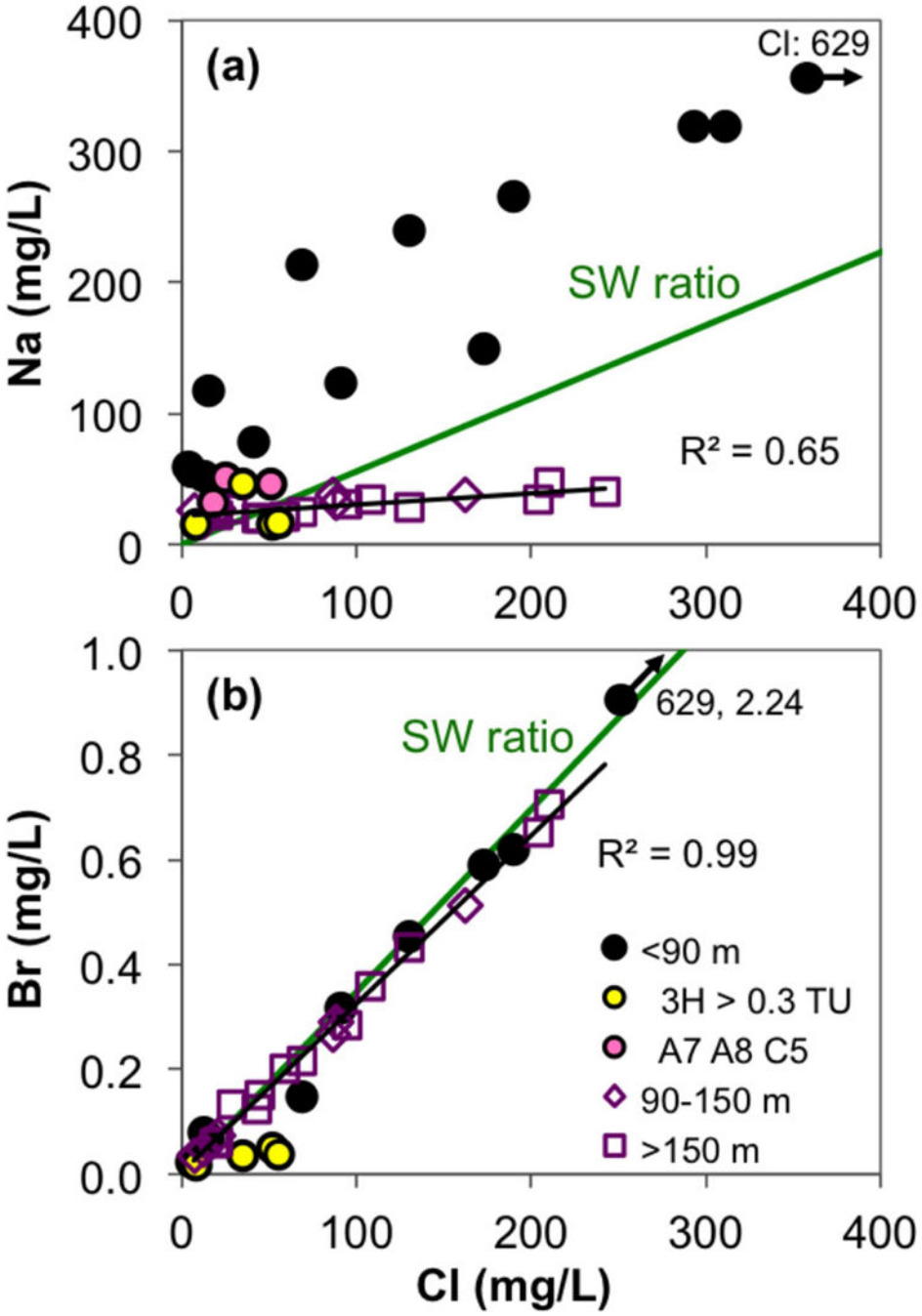

Figure 9.

The correlations of (a) sodium and (b) bromide to chloride. Green lines indicate the trendlines with seawater Na/Cl and Br/Cl ratios. Black lines are the trendlines for pooled intermediate (90–150 m bgl) and deep aquifer (>150 m bgl) groundwater samples. The high Cl sample in (a) actually falls on the seawater line.

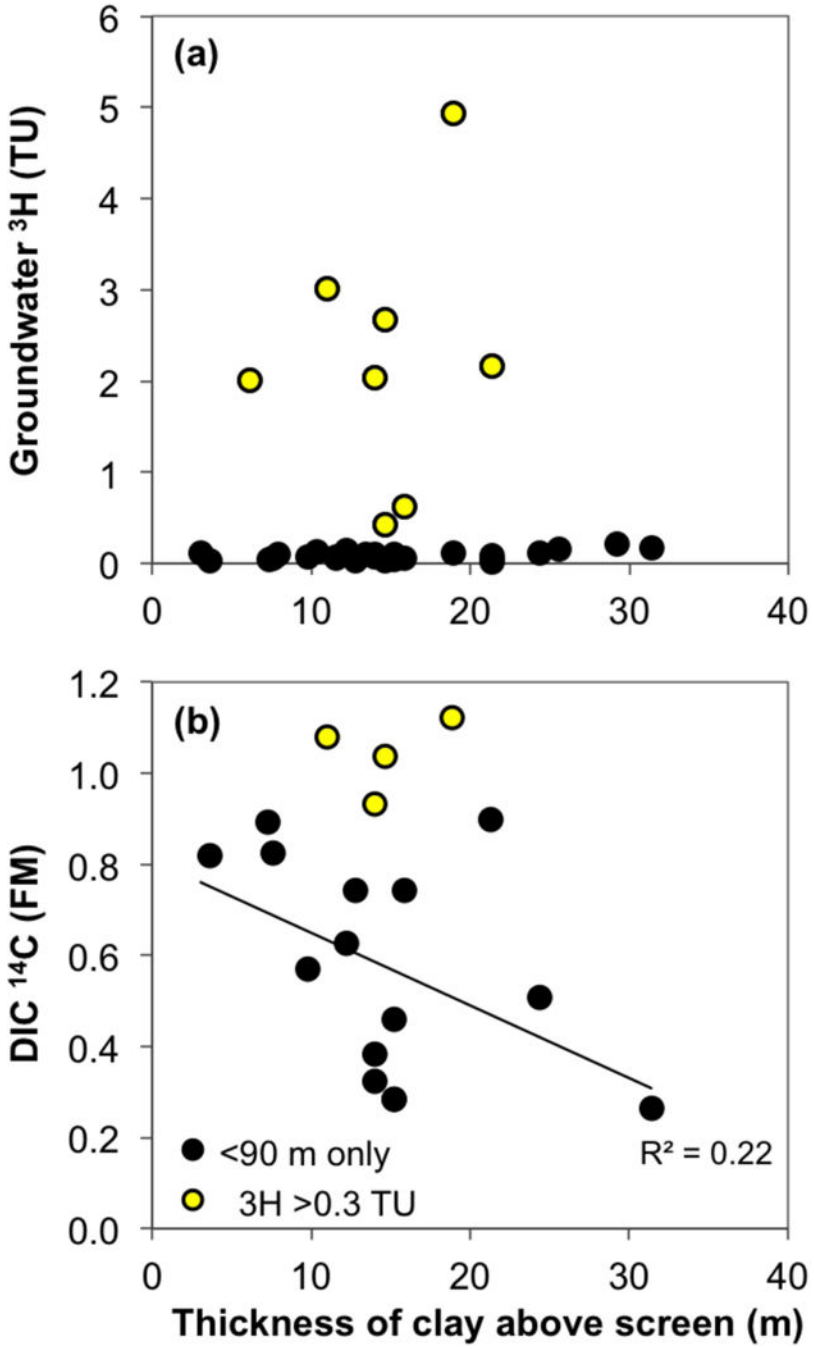

Figure 10.

The relationship between groundwater (a) ^{3}H and (b) ^{14}C vs. the total thickness of clay in lithologs of the shallow low-As wells. For samples where multiple measurements were made, the latest non-negative values of ^{3}H are shown in (a) and the ^{14}C values from 2010 are displayed in (b). The high ^{3}H samples (>0.3 TU, yellow fill) were excluded from the ^{14}C trendline with clay thickness shown in (b).

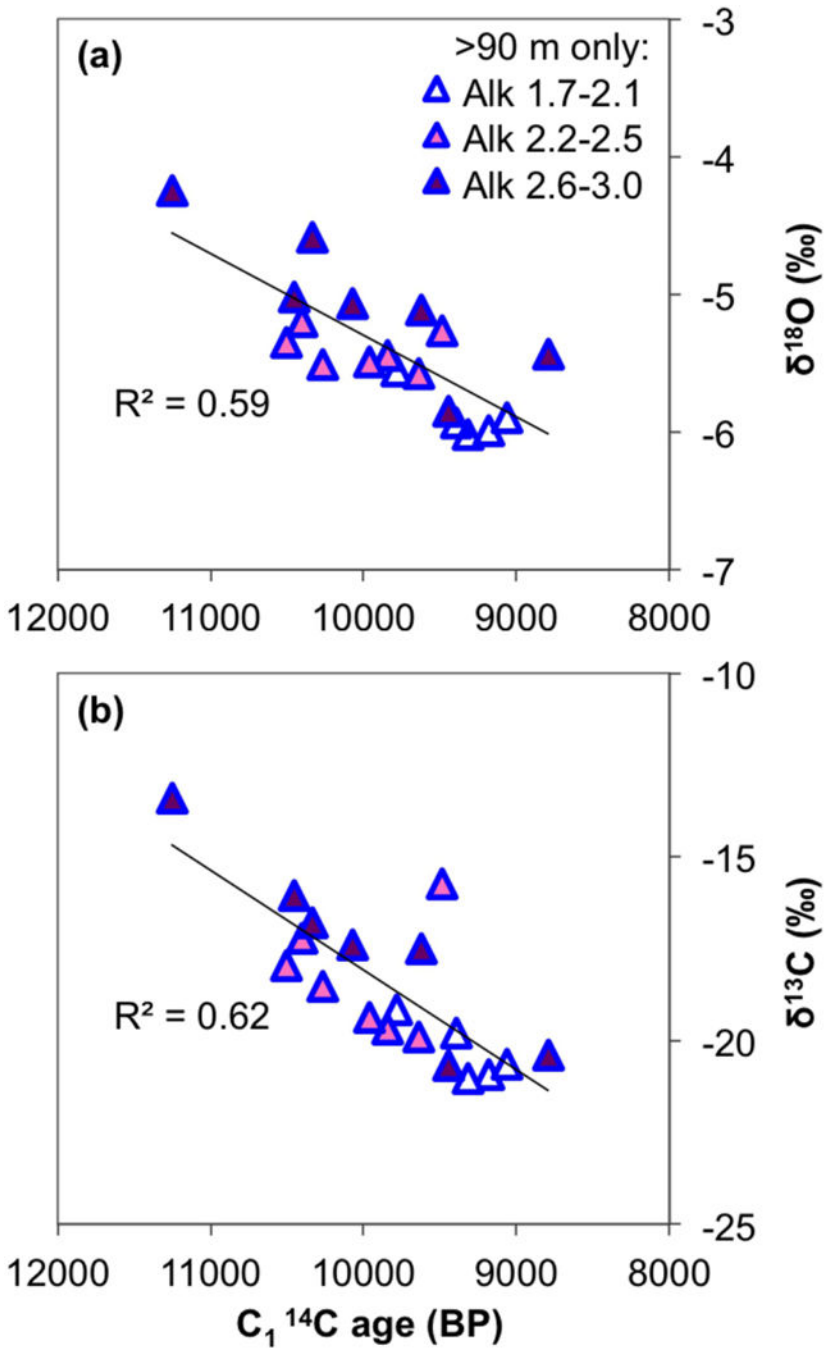

Figure 11.

Plots of (a) $\delta^{18}O$ and (b) $\delta^{13}C_{DIC}$ against the C_1 ^{14}C age in intermediate and deep groundwater only (samples from >90 m bgl), with an added third dimension of alkalinity. The units of alkalinity concentrations shown in the legend are mEq/L, and the three concentration ranges were selected based on the spread of data values. The overall trendlines for pooled intermediate and deep samples and their R^2 values are displayed.

Table 1

Well names, depths, and locations, along with lithological information, ^{3}H and groundwater stable isotope (^{18}O and ^{2}H) concentrations.

Well ID	Depth (m)	Lat (°N)	Long (°E)	Cumm. Clay[a] (m)	Sand color	As (μg/L)	2006 ^{3}H [b] (TU)	± σ (TU)	2010 ^{3}H (TU)	± σ (TU)	2011 ^{3}H (TU)	± σ (TU)	$\delta^{2}H$ (‰)	± σ (‰)	$\delta^{18}O$ (‰)	± σ (‰)
CW28	34.7	23.76845	90.62760	6.1	Orange	–	2.01	0.04								
E5	36.1	23.78999	90.61588	14.6	Orange	2.4	0.03*	0.18					−26.18	1	−4.43	0.1
A7	40.7	23.78534	90.60322	15.2	Orange	0.0	−0.30*	n/a					−33.28	1	−5.20	0.1
CW39	42.7	23.76458	90.59310	15.8	Orange	–	0.63	0.04					−37.41	1	−5.60	0.1
CW27	45.7	23.76813	90.62888	18.9	Orange	0.0	6.15	0.13	4.44	0.08	4.94	0.10	−21.56	0.04	−3.68	0.02
CW23	45.7	23.78743	90.61733	11.0	Orange	0.1	3.36	0.07	3.01	0.06			−12.83	0.08	−2.22	0.02
CW9	45.7	23.78614	90.62142	14.6	Orange	–	0.42	0.05								
CW24	48.8	23.78139	90.61780	29.3	Orange	–	0.21	0.05								
CW37	48.8	23.76285	90.61137	18.3	Orange	–	−0.01	0.03								
G5	49.8	23.77376	90.60069	12.2	Orange	6.6	0.12*	0.05					−38.06	1	−6.01	0.1
C5	52.2	23.78955	90.61113	31.4	Orange	2.9	0.17*	0.18					−32.44	1	−5.11	0.1
CW14	53.3	23.76468	90.60143	12.8	Orange	0.5	0.06	0.03			0.03	0.03	−34.02	0.05	−5.45	0.02
CW16	53.3	23.76574	90.59781	13.4	Orange	–	0.10	0.04								
CW8	55.5	23.77374	90.59457	11.6	Orange	–	0.08	0.03								
CW11	56.1	23.77347	90.64032	21.3	Brownish-grey	–	2.17	0.16								
CW29	56.4	23.76932	90.62417	14.0	Orange	0.4	0.15	0.03	0.07	0.03			−28.89	0.06	−4.82	0.02
F5	57.9	23.77364	90.60453	15.2	Orange	1.0	0.05*	0.05					−39.78	1	−5.95	0.1
CW31	57.9	23.76812	90.62185	14.0	Yellowish-grey	0.3	0.10	0.03	−0.03	0.02			−28.95	0.01	−4.78	0.00
DI4	57.9	23.77100	90.60941	7.6	Orange	0.6	0.05^	0.02					−27.65	1	−4.68	0.1
CW6	58.5	23.78060	90.64434	7.9	Orange	–	0.10	0.03								
CW20	58.5	23.77768	90.60592	3.0	Orange	–	0.12	0.03								
CW35	59.1	23.80112	90.63520	21.3	Orange	–	0.08	0.02								
CW32	59.4	23.76968	90.62048	25.6	Orange	–	0.16	0.05								
CW50	59.4	23.77364	90.60453	no data	Orange	–	0.01	0.04								
CW3	59.7	23.78013	90.64050	3.7	Orange	–	−0.03	0.03								
M1.5	60.5	23.77612	90.63238	14.0	Orange	2.2					2.04	0.06	−20.05	0.09	−3.16	0.01
CW10	61.0	23.79000	90.63612	12.2	Orange	–	0.11	0.03								
CW21	61.0	23.77928	90.60805	10.4	Orange	–	0.12	0.04								
CW30	61.0	23.76525	90.61650	21.3	Orange	–	0.04	0.04								
CW15	62.5	23.75635	90.61013	24.4	Orange	0.1	0.08	0.04	0.11	0.05	−0.01	0.03	−36.34	0.09	−5.51	0.03
CW13	62.8	23.75499	90.61245	11.6	Orange	–	0.06	0.03					−32.51	1	−5.21	0.1

Well ID	Depth (m)	Lat (°N)	Long (°E)	Cumm. Clay[a] (m)	Sand color	As (μg/L)	2006 ^{3}H [b] (TU)	± σ (TU)	2010 ^{3}H (TU)	± σ (TU)	2011 ^{3}H (TU)	± σ (TU)	δ^{2}H (‰)	± σ (‰)	δ^{18}O (‰)	± σ (‰)
CW19	62.8	23.77703	90.59895	18.9	Orange	–	0.12	0.02								
CW17	63.4	23.77158	90.59070	12.2	Orange	–	0.15	0.05					−40.51	1	−5.95	0.1
CW18	64.0	23.77413	90.59233	9.8	Orange	9.4	0.06	0.02	−0.02	0.03	0.08	0.04	−31.95	0.04	−5.20	0.03
CW22	64.0	23.78395	90.61327	14.6	Orange	0.0			2.67	0.06			−21.27	0.03	−3.77	0.02
CW4	65.2	23.78108	90.63325	15.8	Brownish-grey	29.1	0.01	0.03	0.05	0.02			−32.13	0.05	−5.15	0.01
CW25	70.1	23.77623	90.61705	3.7	Yellowish-grey	16.9	0.27	0.04			0.03	0.04	−24.52	0.11	−4.35	0.03
CW33	70.1	23.78758	90.62680	no data	Orange	–	0.17	0.04								
CW38	78.0	23.76919	90.58512	no data	Orange	–	0.14	0.03								
A8	81.5	23.78534	90.60322	15.2	Orange	1.0	0.10*	n/a								
CW12	87.2	23.77612	90.63238	21.3	Grey	0.4			0.02	0.03	0.02	0.03	−21.35	0.04	−3.67	0.03
B CW2	88.5	23.78036	90.63856	7.3	Grey	11.0	0.05	0.09					−26.11	1	−3.13	0.1
CW34	103.6	23.79025	90.63115	28.0	Orange	–	0.17	0.04								
CW41	121.9	23.79158	90.65763	31.7	Orange	–	0.23	0.05					−35.95	1	−5.62	0.1
CW7	123.1	23.78822	90.65173	23.2	Orange	–	0.17	0.04								
CW46	128.0	23.79188	90.61815	12.2	Orange	1.3			−0.01	0.03			−26.95	0.03	−4.58	0.02
CW42	128.0	23.79463	90.65992	18.3	Orange	0.2					0.05	0.03	−37.60	0.08	−5.99	0.02
CW45	129.5	23.78267	90.64853	12.2	Orange	3.6	0.10	0.03	0.01	0.02			−32.75	0.24	−5.35	0.05
CW47	137.2	23.79475	90.65147	18.3	Orange	1.8	−0.06	0.04	0.03	0.02			−36.47	0.13	−5.85	0.01
CW5	141.4	23.77305	90.63365	2.4	Orange	–	0.11	0.03								
CW36	149.4	23.79062	90.62635	6.7	Orange	1.0			0.09	0.03	0.02	0.04	−31.17	0.07	−5.11	0.02
CW44	152.4	23.78500	90.64982	21.3	Orange	6.7			0.06	0.02			−33.76	0.12	−5.50	0.02
WAB24030	205.4	23.75098	90.63160	no data	Orange	8.7			0.03	0.03			−32.26	0.04	−5.26	0.03
WAB24529	219.5	23.78147	90.63872	no data	Orange	0.7					0.04	0.04	−30.26	0.00	−5.02	0.00
WAB24509	222.5	23.76812	90.58532	no data	Orange	0.3					0.00	0.03	−33.70	0.01	−5.43	0.01
WAB24522	225.6	23.79296	90.64467	no data	Orange	0.4					0.01	0.03	−34.51	0.08	−5.56	0.02
WAB24531	231.6	23.77832	90.64477	no data	Whitish-gray	0.6					0.04	0.03	−24.34	0.05	−4.25	0.01
WAB24501	231.6	23.78110	90.64968	no data	Orange	0.9					0.01	0.04	−31.75	0.02	−5.20	0.00
WAB24527	231.6	23.78598	90.65933	no data	Orange	1.4					−0.01	0.03	−33.49	0.06	−5.44	0.00
WAB24538	232.3	23.78538	90.65800	no data	Whitish-grey	1.4					0.04	0.03	−34.29	0.09	−5.57	0.01
WAB24511	234.7	23.78545	90.62695	no data	Orange	1.6					0.04	0.03	−30.58	0.05	−5.06	0.02
WAB24504	234.7	23.79211	90.65718	no data	Orange	1.6					0.00	0.04	−36.97	0.07	−5.93	0.02
WAB24528	234.7	23.78707	90.65923	no data	Whitish-grey	1.7					0.07	0.04	−33.87	0.01	−5.49	0.00
WAB24513	237.7	23.79385	90.65831	no data	Whitish-grey	1.8					0.04	0.04	−37.80	0.03	−6.02	0.01

Well ID	Depth (m)	Lat (°N)	Long (°E)	Cumm. Clay[a] (m)	Sand color	As (μg/L)	2006 ^{3}H [b] (TU)	± σ (TU)	2010 ^{3}H (TU)	± σ (TU)	2011 ^{3}H (TU)	± σ (TU)	δ^{2}H (‰)	± σ (‰)	δ^{18}O (‰)	± σ (‰)
WAB24502	237.7	23.79117	90.66017	no data	Whitish-grey	1.8					0.06	0.03	−37.29	0.03	−5.90	0.01

[a] Cummulative thickness of silt and clay layers above well filter, excluding the top soil

[b] Sampled for ^{3}H in 2003 (*) or 2008 (ˆ)

" – " indicates no measurement was performed; n/a = not available

Table 2

Radiocarbon and ^{13}C data, with calculated ^{14}C ages[a]

Well ID	Depth (m)	As (μg/L)	Phase	FM ^{14}C[b]	± σ (FM)	$\delta^{13}C$	UC ^{14}C age	C_1 ^{14}C age	C_2 ^{14}C age	$\Delta^{14}C$	Accession #
A7	40.7	0.0	DIC	0.2843	n/a	−19.0	10,400	9,530	7,260	−721.0	n/a
CW27 (2010)	45.7	0.0	DIC	1.1216	0.0040	−18.3	Modern[c]	Modern	Modern	113.5	OS-80269
CW27 (2011)	‖	n/ap	DIC	1.1165	0.0036	−18.3	Modern	Modern	Modern	108.3	OS-87014
CW23	45.7	0.1	DIC	1.0792	0.0029	−17.6	Modern	Modern	Modern	71.4	OS-80003
G5	49.8	6.6	DIC	0.6266	n/a	−21.6	3,860	2,990	1,790	−369.5	n/a
C5	52.3	2.9	DIC	0.2631	n/a	−17.6	11,040	10,170	7,250	−735.2	n/a
CW14	53.3	0.5	DIC	0.7419	0.0024	−18.6	2,470	1,600	Modern	−263.5	OS-87015
CW29	56.4	0.4	DIC	0.3841	0.0022	−21.7	7,910	7,040	5,880	−618.7	OS-80000
F5	57.9	1.0	DIC	0.4600	0.0020	−25.9	6,430	5,560	5,860	−542.5	OS-41275
F5	‖	n/ap	DOC	0.5010	0.0030	n/a	5,710	n/ap	n/ap	−502.0	n/a
CW31	57.9	0.3	DIC	0.3238	0.0014	−20.8	9,320	8,450	6,910	−678.6	OS-80004
DI4	57.9	0.6	DIC	0.8259	0.0031	−17.8	1,580	710	Modern	−179.9	OS-68866
M1.5	60.5	2.2	DIC	0.9312	0.0030	−16.6	590	Modern	Modern	−75.6	OS-90066
M1.5	‖	n/ap	DOC	0.8259	0.0021	−24.9	1,580	n/ap	n/ap	−180.3	OS-101857
CW15 (2010)	62.5	0.1	DIC	0.5064	0.0017	−19.9	5,620	4,750	2,850	−497.3	OS-80002
CW15 (2011)	‖	n/ap	DIC	0.5027	0.0028	−19.8	5,690	4,810	2,880	−501.0	OS-87016
CW18 (2010)	64.0	9.4	DIC	0.5692	0.0023	−19.0	4,660	3,790	1,540	−434.9	OS-79994
CW18 (2011)	‖	n/ap	DIC	0.6628	0.0025	−18.4	3,400	2,530	Modern	−342.1	OS-87124
CW18 (2010)	‖	n/ap	DOC	0.4436	0.0020	−26.5	6,720	n/ap	n/ap	−559.6	OS-80285
CW22	64.0	0.0	DIC	1.0374	0.0030	−18.5	Modern	Modern	Modern	29.9	OS-79996
CW4	65.2	29.1	DIC	0.7429	0.0023	−21.9	2,460	1,590	490	−262.4	OS-79992
CW4	‖	n/ap	DOC	0.7521	0.0041	−24.3	2,360	n/ap	n/ap	−253.3	OS-80290
CW25	70.1	16.9	DIC	0.8199	0.0025	−15.7	1,640	770	Modern	−186.1	OS-87122
A8	81.5	1.0	DIC	0.2842	n/a	−19.1	10,400	9,530	7,290	−721.0	n/a
CW12 (2010)	87.2	0.4	DIC	0.8992	0.0029	−16.3	880	Modern	Modern	−107.3	OS-80268
CW12 (2011)	‖	n/ap	DIC	0.9096	0.0029	−16.3	780	Modern	Modern	−97.0	OS-87013
CW12 (2011)	‖	n/ap	DOC	0.7373	0.0022	n/a	2,520	n/ap	n/ap	−268.1	OS-86918
B CW2	88.5	11.0	DIC	0.8940	n/a	−19.2	930	60	Modern	−100.4	n/a

Well ID	Depth (m)	As (μg/L)	Phase	FM $^{14}C^{b}$	± σ (FM)	$\delta^{13}C$	UC ^{14}C age	C_1 ^{14}C age	C_2 ^{14}C age	$\Delta^{14}C$	Accession #
CW46	128.0	1.3	DIC	0.2578	0.0013	−16.8	11,210	10,340	7,050	−744.1	OS-79995
CW42	128.0	0.2	DIC	0.2965	0.0017	−20.9	10,050	9,180	7,710	−705.7	OS-87052
CW45	129.5	3.6	DIC	0.2526	0.0016	−18.0	11,370	10,500	7,760	−749.2	OS-79998
CW47	137.2	1.8	DIC	0.2872	0.0012	−20.7	10,310	9,440	7,870	−714.9	OS-79855
CW36 (2010)	149.4	1.0	DIC	0.2809	0.0013	−17.5	10,500	9,630	6,680	−721.2	OS-79997
CW36 (2011)	‖	n/ap	DIC	0.2636	0.0014	−17.8	11,020	10,150	7,320	−738.4	OS-87123
CW44	152.4	6.7	DIC	0.2600	0.0012	−18.5	11,140	10,260	7,780	−741.9	OS-79856
WAB24030	205.4	8.7	DIC	0.2856	0.0016	−15.7	10,360	9,490	5,660	−716.4	OS-79999
WAB24529	219.5	0.7	DIC	0.2540	0.0018	−16.1	11,330	10,460	6,800	−747.8	OS-87239
WAB24509	222.5	0.3	DIC	0.3106	0.0022	−20.4	9,670	8,790	7,120	−691.7	OS-87236
WAB24522	225.6	0.4	DIC	0.2757	0.0017	−19.2	10,650	9,780	7,580	−726.4	OS-87248
WAB24531	231.7	0.6	DIC	0.2307	0.0013	−13.4	12,120	11,250	6,100	−771.0	OS-87238
WAB24501	231.7	0.9	DIC	0.2558	0.0014	−17.2	11,270	10,400	7,320	−746.1	OS-87252
WAB24527	231.7	1.4	DIC	0.2737	0.0018	−19.7	10,710	9,840	7,870	−728.3	OS-87240
WAB24538	232.3	1.4	DIC	0.2804	0.0020	−19.9	10,510	9,640	7,760	−721.6	OS-87245
WAB24511	234.7	1.6	DIC	0.2660	0.0013	−17.4	10,950	10,080	7,090	−736.0	OS-87237
WAB24504	234.7	1.6	DIC	0.2889	0.0014	−19.8	10,260	9,390	7,470	−713.2	OS-87254
WAB24528	234.7	1.7	DIC	0.2698	0.0015	−19.4	10,830	9,960	7,850	−732.2	OS-87246
WAB24513	237.7	1.8	DIC	0.2916	0.0018	−21.1	10,190	9,320	7,890	−710.5	OS-87258
WAB24502	237.7	1.8	DIC	0.3007	0.0017	−20.6	9,930	9,060	7,470	−701.5	OS-87253

[a] ^{14}C ages were calculated as described in section 3.2. C_1 and C_2 ages are not applicable to DOC ("-")

[b] FM stands for fraction modern radiocarbon

[c] Age is reported as "Modern" when FM≥1 or the age correction resulted in a negative age

‖ = same depth as above; n/ap = not applicable ; n/a = not available

Table 3

Noble gas concentrations and the resulting model recharge temperatures and He surplus (radiogenic He) concentrations[a]

Well ID	Depth (m)	He ccSTP g^{-1}_{GW}	Ne ccSTP g^{-1}_{GW}	Ar ccSTP g^{-1}_{GW}	Kr ccSTP g^{-1}_{GW}	Xe ccSTP g^{-1}_{GW}	$^3He/^4He$	Model prob. (%)[b]	Model T (°C)	err Model T (°C)	He surplus[c] ccSTP g^{-1}_{GW}	He surp.ccSTP g^{-1}_{GW}
E5	36.2	4.00E-08	1.29E-07	2.40E-04	5.51E-08	7.73E-09	1.27E-06	0				
A7	40.7	7.96E-08	2.12E-07	3.22E-04	6.92E-08	9.17E-09	9.09E-07	98.4	22.26	0.65	2.71E-08	1.72E-09
CW27 (2010)	45.7	5.46E-08	2.20E-07	3.17E-04	6.65E-08	8.29E-09	2.75E-06	54.9	31.95	3.44	−1.55E-09	1.51E-09
CW27 (2011, 1)	45.7	5.54E-08	2.25E-07	3.20E-04	6.76E-08	8.75E-09	3.07E-06	73.4	24.33	0.68	−9.22E-10	1.31E-09
CW27 (2011, 2)	45.7	5.46E-08	2.24E-07	3.20E-04	6.77E-08	8.73E-09	3.18E-06	59.7	24.40	0.71	−1.47E-09	1.29E-09
CW23	45.7	5.60E-08	2.33E-07	3.35E-04	7.09E-08	8.92E-09	1.54E-06	16.0	25.34	1.34	−2.04E-09	1.28E-09
G5	49.8	5.35E-08	1.47E-07	2.42E-04	5.41E-08	7.32E-09	1.03E-06	0				
CW14	53.3	5.19E-08	1.74E-07	2.65E-04	5.94E-08	8.06E-09	1.25E-06	0				
CW29	56.4	7.25E-08	1.96E-07	2.97E-04	6.40E-08	8.41E-09	9.31E-07	78.2	24.77	0.66	2.37E-08	1.58E-09
CW31	57.9	7.40E-08	1.96E-07	3.00E-04	6.42E-08	8.49E-09	9.05E-07	70.0	24.65	0.75	2.51E-08	1.59E-09
CW15 (2010)	62.5	5.01E-08	1.03E-07	1.64E-04	3.78E-08	5.56E-09	8.15E-07	0				
CW15 (2011, 1)	62.5	4.71E-08	9.88E-08	1.63E-04	3.72E-08	5.48E-09	8.76E-07	0				
CW15 (2011, 2)	62.5	4.77E-08	9.73E-08	1.59E-04	3.73E-08	5.52E-09	8.38E-07	0				
CW18 (2010)	64.0	5.49E-08	1.72E-07	2.80E-04	6.07E-08	8.00E-09	1.07E-06	0.1				
CW18 (2011)	64.0	5.28E-08	1.82E-07	2.88E-04	6.32E-08	8.45E-09	N/A[d]	82.1	24.15	0.50	7.98E-09	1.35E-09
CW22	64.0	5.71E-08	2.22E-07	3.21E-04	6.71E-08	8.58E-09	1.69E-06	82.1	25.88	1.04	1.33E-09	1.30E-09
CW4	65.2	4.77E-08	1.84E-07	2.93E-04	6.41E-08	8.21E-09	1.15E-06	1.7	25.51	7.87	1.58E-09	1.72E-09
CW25	70.1	5.68E-08	2.13E-07	3.17E-04	6.78E-08	9.15E-09	1.51E-06	36.0	22.03	0.50	3.48E-09	1.46E-09
CW12 (2010)	87.2	5.16E-08	2.09E-07	3.06E-04	6.54E-08	8.22E-09	1.09E-06	20.0	30.92	2.74	−1.47E-09	1.38E-09
CW12 (2011, 1)	87.2	5.32E-08	2.05E-07	3.03E-04	6.53E-08	8.64E-09	1.27E-06	95.1	23.74	0.52	1.76E-09	1.38E-09
CW12 (2011, 2)	87.2	5.34E-08	2.09E-07	3.05E-04	6.54E-08	8.74E-09	1.42E-06	48.9	23.55	0.51	1.02E-09	1.42E-09
CW46	128.0	8.45E-08	2.24E-07	3.26E-04	6.94E-08	8.83E-09	8.77E-07	18.7	24.66	0.98	2.85E-08	1.80E-09
CW42	128.0	7.40E-08	2.12E-07	3.17E-04	6.81E-08	9.39E-09	1.09E-06	3.4	21.22	0.48	2.17E-08	1.78E-09
CW45	129.5	8.02E-08	2.26E-07	3.27E-04	6.97E-08	8.73E-09	9.42E-07	25.2	31.42	2.56	2.28E-08	1.87E-09
CW47	137.2	7.34E-08	2.16E-07	3.23E-04	6.87E-08	8.90E-09	1.02E-06	75.0	24.16	1.04	1.97E-08	1.58E-09
CW36 (2010)	149.4	7.84E-08	2.26E-07	3.28E-04	7.02E-08	8.71E-09	9.70E-07	8.9	30.83	2.88	2.12E-08	1.86E-09
CW36 (2011)	149.4	7.69E-08	2.27E-07	3.25E-04	6.95E-08	9.42E-09	1.04E-06	13.7	21.32	0.49	2.02E-08	1.86E-09

Well ID	Depth (m)	He ccSTP g^{-1}_{GW}	Ne ccSTP g^{-1}_{GW}	Ar ccSTP g^{-1}_{GW}	Kr ccSTP g^{-1}_{GW}	Xe ccSTP g^{-1}_{GW}	$^3He/^4He$	Model prob. (%)[b]	Model T (°C)	err Model T (°C)	He surplus[c] ccSTP g^{-1}_{GW}	He surp.ccSTP g^{-1}_{GW}
CW44	152.4	8.05E-08	2.26E-07	3.21E-05	6.90E-08	8.62E-09	8.91E-07	0				
WAB24030	205.4	8.03E-08	2.28E-07	3.28E-04	7.02E-08	8.97E-09	9.52E-07	15.0	23.59	0.74	2.34E-08	1.74E-09

Grey shading indicates samples that were not used for plots and discussion due to: low model probability and/or model T error >1.5 °C

[a] The model used is described in section 2.3.3.

[b] The probability that model is consistent with the data (>1% is minimum, >5% is a strong criterion)

[c] He surplus is equivalent to radiogenic He

[d] $^3He/^4He$ ratio measurement not available